

ARTICLE OPEN



BDNF restores impaired long-term potentiation of GABAergic synapses induced by chronic ethanol exposure in the VTA and attenuates reward-seeking behavior

Jun-Wei Xiong¹, Meng-Yao Dou¹, Ying Wang^{1,2}, Ting Zeng^{1,2}, Xunzhong Qi³, Jia-Ning Wei¹, Xiao-Wei Shi¹, Dan-Dan Cui¹, Hui-Zhen Dai¹, Chen-Yu Du¹, Xiang-Min Xu¹, Xiao-Fei Wang¹, Xiaofeng Zhu^{1,2,4} and Yanzhong Guan^{1,2,4}

© The Author(s) 2026

Cellular and synaptic plasticity in ventral tegmental area (VTA) play a key role in alcohol use disorder (AUD). Here, we first delineated the *in vivo* dynamics of dopamine (DA) neuron activity in VTA during chronic intermittent ethanol exposure: initial sensitization was followed by a phase of attenuated and dysregulated response upon the first high-concentration exposure, culminating in stable hyper-responsiveness. Chronic ethanol exposure impaired long-term potentiation of GABAergic synapses (LTP_{GABA}) on VTA DA neurons by reducing presynaptic GABA release, and induced lower levels of brain-derived neurotrophic factor (BDNF) expression in VTA. The impaired LTP_{GABA} recovered after 7 days of withdrawal, in parallel with a restoration of BDNF expression in the VTA. Using a combination of pharmacological and region-specific genetic knockdown approaches, we demonstrate that BDNF signaling through its receptor TrkB is both necessary and sufficient for LTP_{GABA} induction. Crucially, in VTA slices from chronic ethanol-exposed mice, BDNF application rescued the impaired LTP_{GABA}. *In vivo*, microinjection of BDNF into the VTA rapidly restored the hyperactive state of DA neuron activity induced by ethanol consumption (6 mice per group), an effect that was mimicked by the GABA_A receptor agonist muscimol and blocked by co-administration of either the TrkB antagonist K252a or the GABA_A receptor antagonist Gabazine. Furthermore, BDNF microinjection significantly attenuated cue-driven ethanol-seeking behavior (reducing the progressive ratio breakpoint by 52%; 6 mice per group), an effect depending on TrkB activation. Together, our findings reveal that chronic ethanol exposure impairs GABAergic plasticity via BDNF-TrkB signaling, while BDNF restores the impaired LTP_{GABA} and dynamics of DA neuron activity, and attenuates ethanol seeking, identifying a novel therapeutic target for AUD.

Molecular Psychiatry; <https://doi.org/10.1038/s41380-026-03532-4>

INTRODUCTION

Alcohol use disorder (AUD) is a prevalent mental health condition characterized by compulsive, heavy drinking and the inability to control alcohol consumption [1]. A core feature of addiction involves the persistent memory of drug-associated “pleasure” and the high propensity for relapse triggered by drug-related cues, which are thought to be caused by maladaptive synaptic plasticity within critical reward circuits [2]. The ventral tegmental area (VTA), a crucial region for reward processing and motivation, plays a central role in the development and maintenance of AUD [3, 4]. Although it is well established that alcohol hijacks synaptic plasticity in the VTA, the precise cellular and molecular mechanisms underlying chronic ethanol-induced adaptations remain poorly understood.

Substantial evidence indicates that long-term changes in synaptic strength, such as long-term potentiation (LTP) and depression (LTD), are involved in the neurobiological basis for learning, memory, and addictive behaviors [5]. Acute ethanol exposure increases the firing rate of midbrain dopaminergic neurons and elevates dopamine levels [6]. Acute ethanol also

disrupts various forms of LTP across multiple brain regions, including kainate receptor-dependent LTP in the basolateral amygdala [7], N-methyl-d-aspartate receptor (NMDAR)-dependent LTP in the prefrontal cortex (PFC) [8], and NMDAR-dependent LTP in the hippocampal CA1 region [9]. Acute ethanol likewise impairs metabotropic glutamate receptor-dependent LTP in the nucleus accumbens (NAc) core [10], while paradoxically inducing LTP via GluN2B NMDAR in the dorsal striatum [11]. Our previous studies demonstrated that acute ethanol exposure inhibits long-term potentiation of GABAergic synapses (LTP_{GABA}) onto dopamine (DA) neurons in VTA [12], where LTP_{GABA} normally acts as a “brake” on dopaminergic neuron activity [13, 14]. These findings collectively suggest that dysregulation of synaptic potentiation may contribute critically to AUD. However, while acute effects are increasingly documented, how chronic ethanol exposure alters GABAergic plasticity in the VTA remains largely unexplored.

Brain-derived neurotrophic factor (BDNF) is a widely studied neurotrophin, which plays a pivotal role in neuronal development, synaptic plasticity, and the pathophysiology of psychiatric disorders [15–17]. BDNF is known to mediate activity-dependent

¹Department of Physiology and Neurobiology, Institute of Brain Science, Mudanjiang Medical University, Mudanjiang, China. ²Heilongjiang Province Key Laboratory of Mechanism and Prevention of Substance Dependence Disease, Mudanjiang, China. ³Department of Neurology, the First Affiliated Hospital of Jiamusi University, Jiamusi, China. ⁴Development and Application of North Traditional Chinese Medicine Collaborative Innovation Center in Mudanjiang, Mudanjiang, China. ✉email: guanyz@mdjmu.edu.cn

Received: 24 July 2024 Revised: 10 February 2026 Accepted: 10 March 2026

Published online: 23 March 2026

LTP in the hippocampus and other regions [18]. Both BDNF and its high-affinity receptor, tropomyosin receptor kinase B (TrkB), are abundantly expressed along the mesocorticolimbic dopamine pathway [19, 20] and are closely associated with addiction-related behaviors [21–23]. We newly report that chronic ethanol exposure decreases BDNF expression in the VTA, and that local administration of BDNF or a TrkB agonist decreases ethanol intake and alleviates symptoms of ethanol withdrawal [24, 25]. However, BDNF exerts region-specific, and sometimes opposing effects, on drug seeking: BDNF promotes cocaine-seeking when injected into the NAC [26], suppresses drug seeking when delivered into the PFC [27], and induces an opiate-like reward state in the VTA [28]. These divergent outcomes underscore the importance of defining circuit-specific roles of BDNF in drug addiction. Given the role of BDNF in regulating synaptic strength [29, 30] and its lower levels of expression in the VTA following chronic ethanol [25], we postulated that BDNF-TrkB signaling may serve as a critical link between ethanol exposure and GABAergic plasticity. Specifically, we hypothesized that the loss of BDNF signaling contributes to the impaired LTP_{GABA}, thereby removing a key inhibitory constraint on VTA DA neurons and promoting maladaptive ethanol-related behaviors.

In this study, we first employed *in vivo* fiber photometry to characterize the dynamic trajectory of VTA DA neuron activity throughout chronic intermittent alcohol exposure. We then combined *ex vivo* electrophysiology, molecular biology, pharmacological methods, and region-specific genetic knockdown to test whether chronic ethanol disrupts LTP_{GABA} via the BDNF-TrkB, and if restoring this molecular pathway can rescue the impaired synaptic plasticity and dynamics of DA neuron activity, and attenuate alcohol-seeking behavior at last.

MATERIALS AND METHODS

Animals

All experimental procedures were approved by the Institutional Animal Care and Use Committee of Mudanjiang Medical University. To minimize the effects of sex hormones like estrogen [31], oxytocin [32], and to limit the impact of ethanol on synaptic plasticity across developmental stages [33, 34], we employed 8-week-old adult male mice. Wild-type C57BL/6J mice were obtained from the Center for Comparative Medicine of Mudanjiang Medical University (SYXK(Hei)2024-015). DAT-IRES-Cre mice (on a C57BL/6J background) were provided by Changzhou Cavens Laboratory Animal Co., Ltd. (SCXK(Su)2021-0013). All mice were group-housed under standard specific-pathogen-free conditions with a 12-h light/dark cycle, ambient temperature of 22–25 °C, and humidity of 50 ± 10%. They had *ad libitum* access to standard laboratory chow (LAD 10000 M) and water. Sample sizes for animal experiments were determined based on established protocols from prior studies investigating similar behavioral paradigms.

Chemicals and reagents

The majority of chemical reagents were sourced from Sigma-Aldrich (St. Louis, USA) and Tocris Bioscience (Bristol, UK). Ethanol (95%) was obtained from Henan Hanyong Alcohol Co., Ltd. (Henan, China). Recombinant human BDNF was from Absin Biotechnology (Shanghai, China; catalog #abs04185). The pharmacological agents K252a (catalog #HY-N6732), Muscimol (catalog #HY-N2313), and Gabazine (catalog #HY-103533) were acquired from MedChemExpress (New Jersey, USA). All drugs for microinjection were freshly prepared on the day of the experiment using the vehicles specified in the methods.

Behavioral procedures

Intermittent access to ethanol via a 2-bottle choice (IA2BC). Ethanol solutions (v/v) were prepared by diluting 95% ethanol with tap water. The IA2BC paradigm, adapted from our previous study [35], is illustrated in Fig. 1A. Specifically, adult male C57 mice were individually housed in cages, each equipped with 50-mL centrifuge tubes, which served as drinking vessels with steel ball sippers for water and ethanol. Following a minimum 3-day acclimatization period to the centrifuge tubes, the mice

were offered a 3% ethanol solution and water on day 1. On day 2, the ethanol bottle was replaced with a second water bottle. On day 3, the initial water bottle was replaced with a 6% ethanol solution. This sequence was repeated, gradually increasing the ethanol concentration in increments of 3%, 6%, 10%, and finally 20%. To avoid side bias, bottle placement (left or right) alternated daily. The body weights of the mice were measured weekly, and average weekly “drip” was calculated to adjust for spillage or evaporation (loss of liquid in the cage with no animal present). Ethanol consumption was quantified as follows: Ethanol intake (g/kg/24 h) = [(ethanol intake in grams – “drip” loss in grams) × (ethanol concentration) × (density of ethanol in g/mL)] / (body weight in kg) / 24 h. Ethanol preference was expressed as the percentage of ethanol solution volume consumed relative to the total fluid (ethanol + water) volume intake, expressed as: Ethanol preference (%) = [(ethanol solution volume intake (mL)) / (total fluid intake (mL))] × 100%. Throughout IA2BC, mice had unrestricted access to food and fluids. Following 21 days of IA2BC, mice were randomly assigned to different withdrawal groups (0 hour, 3 days, 7 days) for subsequent ethanol withdrawal-related procedures.

Operant ethanol self-administration. The protocol was adapted from previous studies [36–39]. Overnight training and subsequent experiments were conducted in operant chambers (Skinner box XR-XS109, Shanghai Xinruan Information Technology Co., Ltd., China). Each chamber, with a stainless-steel grid floor and modular test area (22×22×20 cm), was situated within a ventilated, sound-attenuated compartment. The chambers were equipped with 2 pressable stainless-steel levers, each topped with a white cue light. Correct responses triggered liquid reward delivery from a sipper tube via pump. Specifically, pressing the active lever illuminated the cue light for 2000 ms, dispensing approximately 10 µL of liquid over 50 ms, followed by a 5-s timeout during which no responses were required. The VisuTrack software (Shanghai Xinruan Information Technology Co., Ltd., China) was used to log data on session durations, lever presses, reward collections, and cue light activations, among other parameters.

Habituation: overnight training. Mice underwent overnight training (approximately 16 h) in the operant chamber to acclimate to the environment. During this period, the mice could freely explore the chamber and learn to obtain a 10% sucrose solution by pressing the active lever. By contrast, pressing the inactive lever resulted in no programmed consequences. Reward acquisition via lever pressing followed a fixed ratio 1 (FR1) schedule. To ensure adequate energy, food pellets were provided in the chamber throughout the overnight session.

Sucrose fade training. Similar to overnight training, sucrose was gradually replaced to a 10% ethanol solution over 45-min daily sessions of sucrose fading training. The “sucrose fading” protocol was as follows: on days 1–5, 5% sucrose and 5% ethanol; on days 6–8, 2.5% sucrose and 10% ethanol. After complete sucrose phased-out, all sessions used 10% ethanol.

Fixed ratio training. During the daily 45-min fixed ratio (FR) training sessions, the mice initially completed 7 days of training at FR1. Upon achieving stable lever-pressing performance at this ratio, the regimen progressed to 4 days each at FR2, FR3, and FR5. The lever-pressing behavior ultimately stabilized at a baseline response, maintaining an accuracy of at least 0.63.

Progressive ratio training. Following stable FR baseline performance, mice underwent progressive ratio (PR) training to assess the motivation to work for ethanol. The response requirement for each subsequent reward based on the formula: PR = [5e^(0.2^R)] - 5, with “R” representing the sequential number of lever presses required to obtain each reward, starting with R = 1 [40]. This generates an increasing series of response requirements (e.g., 1, 2, 4, 6, 9, 12, 15...). The session continued until the mouse failed to complete a ratio within 45 minutes. The breakpoint (BP), defined as the last successfully completed ratio, was used as the primary measure of the animal’s maximal effort or motivation to seek the ethanol reward [41].

Extinction. During the extinction phase, the protocol closely mirrored that of the FR training period; however, it differed in that cues (lights) and the delivery of rewards (ethanol) following correct lever presses were omitted.

Acute slice preparation

Acute brain slices were prepared following methods adapted from previous studies [42, 43]. Briefly, mice were deeply anesthetized with

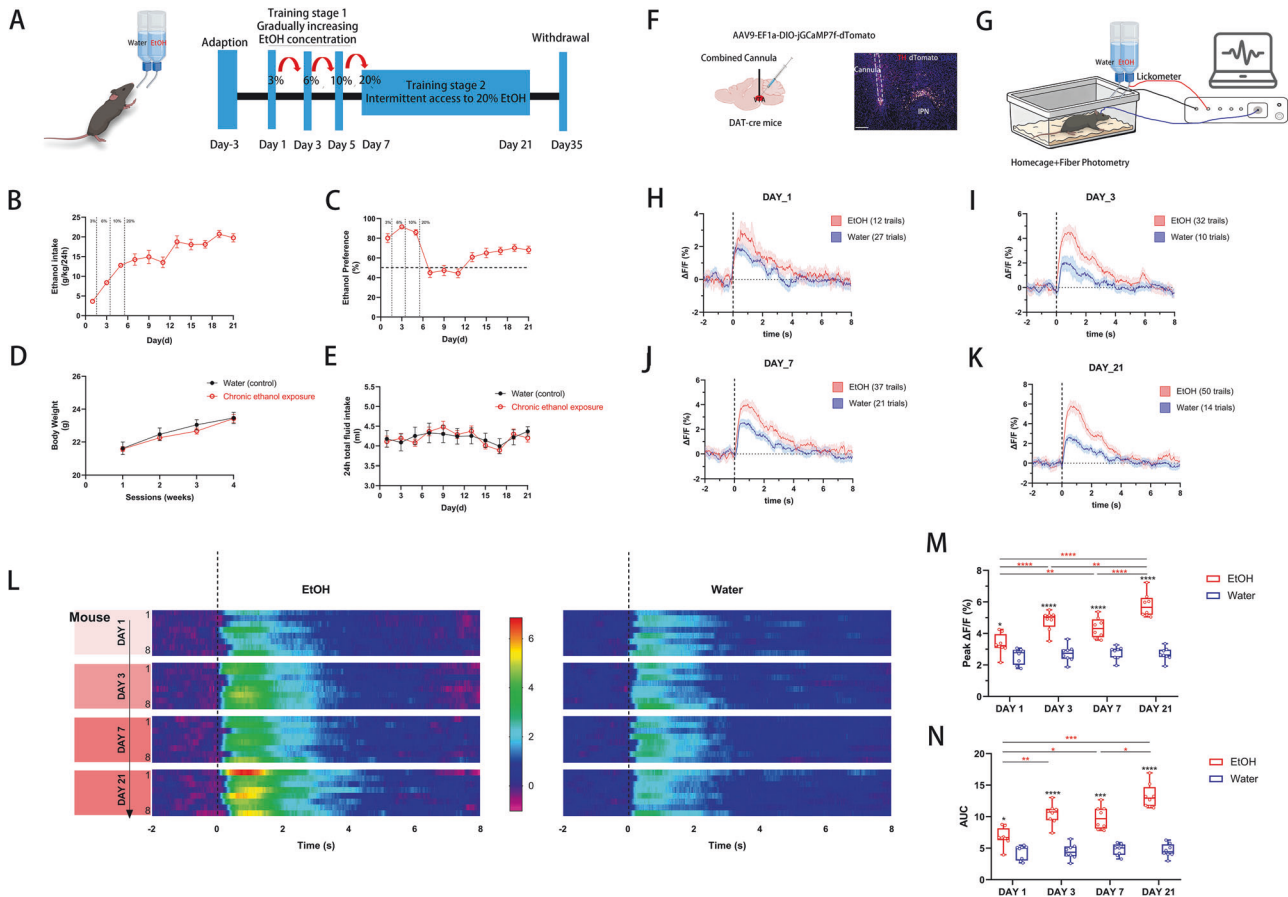


Fig. 1 Chronic Ethanol Exposure Dynamically Reshapes VTA DA Neuron Activity in Vivo. (A) Schematic of the intermittent access two-bottle choice (IA2BC) paradigm. (B) Escalating 24 h ethanol intake across 21 days of IA2BC. Ethanol intake increased from 3.66 ± 0.25 g/kg/24 h on day 1 to 19.78 ± 1.04 g/kg/24 h by day 21 ($n = 24$ mice). (C) Ethanol preference during IA2BC. The average preference over the 21-day period was $68.17 \pm 3.79\%$ ($n = 24$ mice). (D) Total 24 h fluid intake (mL) of IA2BC and water-only control mice. There was no significant difference between groups (Two-way ANOVA, $F(1, 28) = 0.002$, $p > 0.05$; $n = 10$ control mice, $n = 24$ IA2BC mice). (E) Body weight of IA2BC and water-only control mice. There was no significant difference between groups (Two-way ANOVA, $F(1, 28) = 0.28$, $p > 0.05$; $n = 10$ control mice, $n = 24$ IA2BC mice). (F) Schematic of AAV injection for GcAMP7f expression in VTA DA neurons (left). Coronal VTA section showing immunofluorescence for TH (red, DA neurons), expressed GcAMP7f reporter (dTomato, gray), and DAPI (blue). Scale bar, 100 μ m. (G) Schematic of in vivo fiber photometry recording in homecage. Licking events for water or ethanol were detected by lickmeters. (H–K) Representative average calcium transients ($\Delta F/F$) aligned to licking onset (dashed line at 0 s) for ethanol (red) and water (blue) from a single mouse on Day 1 (H), Day 3 (I), Day 7 (J), and Day 21 (K). Traces represent mean \pm SEM of all trials from one representative animal per time point. (L) Population heatmaps of $\Delta F/F$ responses (aligned to lick onset, dashed line) for all recorded mice. Left: Ethanol licking events. Right: Water licking events. Each row represents the average response of one mouse ($n = 8$ mice per time point). (M) Quantification of peak $\Delta F/F$ for ethanol (red) and water (blue) events across the four time points. Two-way ANOVA revealed significant main effects of Day ($F(3, 42) = 15.62$, $p < 0.0001$) and Fluid (Ethanol vs. Water) ($F(1, 14) = 127.1$, $p < 0.0001$), with a significant interaction ($F(3, 42) = 12.90$, $p < 0.0001$). *Post hoc* comparisons (Tukey's test for across-day ethanol; Bonferroni's test for within-day fluid): Ethanol: Day 1 ($3.32 \pm 0.23\%$) vs. Day 3 ($4.82 \pm 0.22\%$), $p < 0.0001$; Day 1 vs. Day 7 ($4.36 \pm 0.23\%$), $p = 0.0027$; Day 1 vs. Day 21 ($5.80 \pm 0.27\%$), $p < 0.0001$; Day 3 vs. Day 21, $p = 0.0047$; Day 7 vs. Day 21, $p < 0.0001$. *Within-day Ethanol vs. Water*: Day 1 (Water: $2.56 \pm 0.18\%$), $p = 0.0426$; Day 3 (Water: $2.72 \pm 0.19\%$), $p < 0.0001$; Day 7 (Water: $2.76 \pm 0.15\%$), $p < 0.0001$; Day 21 (Water: $2.69 \pm 0.15\%$), $p < 0.0001$. Water responses did not differ across days. (N) Quantification of area under the curve (AUC, %·s) for ethanol (red) and water (blue) events. Two-way ANOVA revealed significant main effects of Day ($F(2.80, 39.16) = 16.70$, $p < 0.0001$) and Fluid ($F(1, 14) = 172.0$, $p < 0.0001$), with a significant interaction ($F(3, 42) = 14.21$, $p < 0.0001$). *Post hoc* comparisons (Tukey's test for across-day ethanol; Bonferroni's test for within-day fluid): Ethanol: Day 1 ($6.78 \pm 0.53\%$ -s) vs. Day 3 ($10.42 \pm 0.58\%$ -s), $p = 0.0058$; Day 1 vs. Day 7 ($9.86 \pm 0.64\%$ -s), $p = 0.0168$; Day 1 vs. Day 21 ($13.26 \pm 0.68\%$ -s), $p = 0.0002$; Day 7 vs. Day 21, $p = 0.0187$. *Within-day Ethanol vs. Water*: Day 1 (Water: $4.35 \pm 0.41\%$ -s), $p = 0.0122$; Day 3 (Water: $4.47 \pm 0.42\%$ -s), $p < 0.0001$; Day 7 (Water: $4.79 \pm 0.33\%$ -s), $p = 0.0001$; Day 21 (Water: $4.64 \pm 0.37\%$ -s), $p < 0.0001$. Water responses did not differ across days. All bar/box plots in (M, N) show data from $n = 8$ mice per time point. Data are presented as mean \pm SEM. * $p < 0.05$, ** $p < 0.01$, *** $p < 0.001$, **** $p < 0.0001$.

isoflurane and underwent cardiac perfusion with ice-cold, oxygenated choline-based artificial cerebrospinal fluid (ACSF) containing 120 mM choline chloride, 2.5 mM potassium chloride (KCl), 0.5 mM calcium chloride (CaCl_2), 7 mM magnesium sulfate (MgSO_4), 1.25 mM monosodium phosphate (NaH_2PO_4), 5 mM sodium ascorbate, 3 mM sodium pyruvate, 26 mM sodium bicarbonate (NaHCO_3), and 25 mM glucose. Following perfusion, the brains were rapidly dissected post-decapitation and submerged in ice-cold oxygenated choline-based ACSF. Horizontal slices containing the VTA were accurately cut to a thickness of 220 μ m using a vibratome (VT 1000S, Leica), then incubated in the same oxygenated cutting ACSF at 34 $^\circ\text{C}$ for

15 min. Finally, the slices were allowed to recover at room temperature for at least 1 h in standard ACSF (in mM, 124 sodium chloride (NaCl), 2.5 KCl, 2.5 CaCl_2 , 2 MgSO_4 , 1.25 NaH_2PO_4 , 22 NaHCO_3 , and 10 glucose, pH 7.2–7.3).

Ex vivo electrophysiological recording

Electrophysiological signals were recorded using the MultiClamp 700B amplifier (Molecular Device, San Jose, CA, United States), Digidata 1440 A/A/D converter (Molecular Device), and pCLAMP 10.4 software (Molecular Device). Slices were transferred to a recording chamber where

ACSF perfusion (2 mL/min) and the temperature (32–34 °C) was maintained using a temperature controller (TC-324B, Warner Instruments, Hamden, CT, United States). The medial terminal nucleus of the accessory optic tract served as a distinctive landmark to identify the VTA [44]. Whole-cell recordings were conducted using glass electrodes (2–3 M Ω) filled with internal solution containing (in mM) 130 KCl, 5 NaCl, 1 magnesium chloride, 2 ATP-Na, 0.1 GTP-Na, 0.2 EGTA, and 10 HEPES. Throughout the experiments, series resistance was continuously online monitored, and the cells were excluded from analysis for deviations >20%.

Putative DA neurons within the VTA were characterized by soma size (>20 μ m) and a large I_h current (>100 pA) [45, 46]. Specifically, the steady-state h -current was greater than 100 pA during a voltage step protocol (-70 to -120 mV in 10 mV steps, 1.5 s duration). Furthermore, GABA_A receptor-mediated currents were isolated using 20 μ M CNQX to block synaptic currents mediated by AMPA receptors and 1 μ M strychnine to block synaptic currents mediated by glycine receptors. These currents were then confirmed using 100 μ M PTX, which blocks the GABA_A receptor. VTA DA neurons were voltage-clamped at -70 mV except during high-frequency stimulation (HFS), when neurons were in current-clamp mode so that the HFS trains were delivered with the membrane potential free to vary. Evoked inhibitory postsynaptic current (eIPSCs) was elicited using bipolar stainless steel stimulating electrode, placed approximately 200–500 μ m rostrally to the VTA from the recorded neuron [42]. Stimulus intensities for eIPSC were calibrated to 50–70% of the maximum evoked current to avoid postsynaptic receptor saturation. GABA_A receptor-mediated eIPSCs were elicited at 0.1 Hz for 10 min to establish a baseline prior to HFS. For each neuron, once the stimulus intensity was established, it was maintained constant throughout the recording session. Induction of LTP_{GABA} involved stimulating afferents at 100 Hz for 1 s (HFS); the train was repeated twice, with a 20-s interval between trains. Following HFS, eIPSC recording continued for an additional 30–50 min. Pharmacological treatments including: (1) 200 nM K252a [47], a TrkB antagonist, was added to the incubation solution before HFS, and following 10 min of baseline recording, the perfusion was switched to ACSF without K252a; (2) 200 nM K252a was added after HFS and continued until the end of the recording; (3) 20 ng/mL BDNF [47] was added after baseline recording and continued until the end of the recording; (4) under continuous incubation with K252a, 20 ng/mL BDNF was added after 10 min of baseline recording before HFS.

Data were low-pass filtered at 3 kHz, digitized at 10 kHz, and stored on a computer for subsequent offline analysis using the pCLAMP 10.4 software.

Stereotaxic surgeries and microinjections

Mice were anesthetized with a mixture of xylazine (10 mg/kg) and ketamine (80 mg/kg), and secured in a stereotaxic frame (RWD Life Sciences, China). Body temperature was maintained at 37–38 °C using a heating pad throughout surgery. All coordinates are relative to bregma according to the Franklin and Paxinos mouse brain atlas [48].

Surgeries for viral-mediated gene knockdown (for ex vivo electrophysiology)

For in vivo knockdown of BDNF or TrkB, wild-type mice received bilateral injections of AAV9-CAG-GFP-mir30shrRNA (targeting *BDNF*, *Ntrk2*, or a scrambled control; 1×10^{13} vg/mL, WZ Biosciences, China) into the VTA (AP: -3.2 mm, ML: ± 0.5 mm, DV: -4.5 mm). A volume of 0.4 μ L per side was delivered via a 33-gauge Hamilton syringe at a rate of 0.1 μ L/min. The needle was left in place for 5 min post-injection before withdrawal. Mice were allowed at least 3 weeks for viral expression prior to western blot or slice electrophysiology.

The vectors encoded shRNA targeting mouse *Bdnf* (NCBI RefSeq: NM_007540.4), *Ntrk2* (TrkB; NCBI RefSeq: NM_001025074.1), or a non-targeting scrambled control sequence (AAV9-CAG-GFP-mir30shrRNA; WZ Biosciences, Jinan, China). The proprietary shRNA sequences were designed and validated by the manufacturer. Prior to packaging, candidate shRNAs were screened in HEK293 cells using quantitative RT-PCR, confirming efficient knockdown of target mRNA levels (e.g., reduction to 24–36% of control for *Bdnf* and 29–36% for *Ntrk2* by the most effective constructs). The final selected shRNA sequences are not disclosed as they are part of the company's proprietary RNAi platform. For in vivo validation of knockdown at the protein level in the VTA, please refer to Figs. 5B and 5F. Note on Genotyping: The following primer sequences were used for genotyping and molecular validation of the target genes:

Bdnf: Forward 5'-CATGTACGTTGCTATCCAGGC-3', Reverse 5'-CTCCTTAATGTCACGCACGAT-3'.

Ntrk2: Forward 5'-TGCACTCCGCTAGGATTGG-3', Reverse 5'-GGGTCAACGCTGTAGGTTTC-3'.

Surgeries for in vivo fiber photometry

DAT-Cre mice were used for calcium imaging. They received a unilateral injection of AAV9-EF1a-DIO-jGCaMP7f-P2A-nls-dTomato (1×10^{13} vg/mL, WZ Biosciences, China) into the left VTA (coordinates as above). Immediately following the viral injection (0.4 μ L, 0.1 μ L/min, 5-min delay), a custom combined guide cannula (Suzhou Taohuaduo Biotechnology, China), designed for sequential drug infusion and optical fiber insertion, was implanted at the same coordinates and secured with dental cement. A dummy cannula was inserted for sealing between experiments. Mice recovered for 3 weeks to allow for sufficient viral expression and protein maturation before fiber photometry recordings.

Surgeries and drug microinjection for operant ethanol-seeking behavior

A separate cohort of mice was implanted with bilateral guide cannulas (26 gauge; Plastics One) targeted at the VTA (coordinates as above). These mice were used for the operant self-administration and progressive ratio tests. After a minimum 7-day recovery and subsequent re-establishment of stable lever-pressing performance, they were randomly assigned to receive bilateral intra-VTA drug microinjections. The treatment groups were: Vehicle, BDNF, K252a, and BDNF+K252a. Recombinant human BDNF (0.5 μ g/ μ L, 0.5 μ L/side) [49] was prepared in 0.1% BSA-ACSF. K252a (50 μ M, 0.5 μ L/side) [35] was prepared in 1% DMSO-ACSF. Drugs were infused at 0.1 μ L/min via injection cannulas extending 0.5 mm beyond the guide tip. The cannulas were left in place for an additional 2–5 min post-infusion. PR testing began 30–60 min after microinjection.

Drug microinjection during in vivo fiber photometry recording

For pharmacological experiments during calcium imaging, mice prepared received a unilateral microinjection into the VTA through the combined guide cannula. The treatment groups were: Vehicle, BDNF, Muscimol, BDNF+Gabazine, and BDNF+K252a. BDNF and K252a were prepared as above. Muscimol (GABA_A receptor agonist, 1 μ g/ μ L, 0.5 μ L) and Gabazine (GABA_A receptor antagonist, 0.5 μ g/ μ L, 0.5 μ L) were dissolved in ACSF [50]. Fiber photometry recording commenced 10–15 min after the completion of microinjection.

After completing all operant behavioral tests, mice were microinjected bilaterally with an equal volume of Coomassie brilliant blue dye (0.5 μ L/side) into the VTA. Brains were sectioned, and injection sites were verified by comparison with the stereotaxic atlas. Data from mice with injection sites located outside the VTA were excluded from analysis (4 out of 30 mice; see Supplementary Figure S1 for placement map). These excluded mice showed no significant behavioral response in PR tests, confirming the site-specificity of the drug effects. Injection sites for the photometry cohort were confirmed post-hoc by immunohistochemistry for the viral reporter (dTomato) and tyrosine hydroxylase.

In vivo fiber photometry recording

In vivo calcium signals from VTA DA neurons were recorded in the homecage during specified days (Days 1, 3, 7, 21) of the IA2BC paradigm. Recordings were conducted during the first hour of the drinking session to capture the core phase of 'front-loading' behavior, characterized by rapid, excessive ethanol consumption upon renewed availability [51]. For pharmacological experiments, recordings began 10–15 minutes after intra-VTA microinjection of Vehicle, BDNF, Muscimol, BDNF+Gabazine, or BDNF+K252a.

Licking behavior for ethanol and water was detected in real-time by capacitive touch sensors on custom-made lickometers. The onset of each lick was tagged by a TTL pulse, which was synchronously recorded with the photometry signal to ensure precise temporal alignment between behavior and neural activity. Photometry was performed using a three-color fiber photometry system (Thinker Tech Nanjing Bioscience Inc). Excitation light from 470 nm (for jGCaMP7f) and 405 nm (isosbestic control) LEDs was delivered via a 400 μ m core, 0.48 NA optical fiber. Emitted fluorescence was collected, filtered, and digitized at 40 Hz. Data acquisition and processing were performed using the FiberAnalysis system software (Thinker Tech Nanjing Bioscience Inc). Raw signals were smoothed with a Lowess filter, and $\Delta F/F$ was calculated as $(F_{470} - F_{405})/F_{405}$, using the 405 nm channel to correct for motion and bleaching artifacts. For analysis,

data were segmented into trials aligned to the onset of individual licking events. The mean $\Delta F/F$ during the 2-second window preceding lick onset served as the baseline. From each event-aligned transient, the peak $\Delta F/F$ amplitude and the area under the curve (AUC) within a defined post-lick window were calculated for statistical comparison.

Western blot

After the final behavioral test, mice were anesthetized with isoflurane and decapitated for brain collection. The VTA was rapidly excised from the dissected brain slices in ice-cold ACSF. The bilateral VTA samples were homogenized in ice-cold radioimmunoprecipitation assay lysis buffer (P0013B; Beyotime, China) and then centrifuged at 4 °C and 12000 g for 20 min. Protein concentration was determined using a bicinchoninic acid protein assay kit (P0012; Beyotime, China). Samples containing 20 μ g of protein were electrophoresed on a 12% sodium dodecyl sulfate-polyacrylamide gel, transferred to a polyvinylidene difluoride (PVDF) membrane, and incubated overnight at 4 °C with primary antibodies (rabbit anti-BDNF 1:1000, Abcam, Cat# ab108319; rabbit anti-TrkB 1:1000, Cell Signaling Technology, Cat# 4603; rabbit anti-GAPDH 1:1000, Abcam, Cat# ab181602). The following day, the PVDF membrane was washed 3 times with TBST (10 min each) and then incubated at room temperature for 2 h with horseradish peroxidase-conjugated goat anti-rabbit IgG secondary antibody (1:1000, A0208, Beyotime, China). After 3 more washes with TBST (10 min each), protein detection was performed using the BeyoECL Plus chemiluminescence detection kit (P0018S, Beyotime, China) and visualized with a gel imaging system (AI600, GE, USA). Finally, protein grayscale values were analyzed using the ImageJ software. All results were normalized to 100% based on control group averages.

Immunohistochemistry and imaging

To confirm viral expression, immunohistochemistry was performed. Mice were deeply anesthetized and transcardially perfused with ice-cold phosphate-buffered saline (PBS) followed by 4% paraformaldehyde (PFA) in PBS. Brains were post-fixed in 4% PFA overnight at 4 °C and then transferred to a 30% sucrose solution for cryoprotection. Coronal sections (40 μ m thick) containing the VTA were cut using a vibratome (VT 1000S, Leica). Free-floating sections were permeabilized with 0.3% Triton X-100 (Beyotime, P0096) in PBS for 30 min at room temperature, followed by blocking with 5% normal goat serum (Beyotime, C0265) and 0.1% BSA for 2 hours at room temperature. Sections were then incubated with primary antibodies diluted in blocking solution on a shaker at 4 °C overnight (~16 hours). The following primary antibodies were used: rabbit anti-GFP (1:1000; Proteintech Group, Inc, pabg1), rabbit anti-pan-RFP (1:500 for dTomato detection; Proteintech Group, Inc, pabr1), and mouse anti-tyrosine hydroxylase (TH, 1:500; MedChemExpress, YA5393). After extensive washing with PBST, sections were incubated with corresponding secondary antibodies for 2 hours at room temperature: Alexa Fluor 488-conjugated goat anti-rabbit IgG (1:1000; MedChemExpress, HY-P8002), Alexa Fluor 594-conjugated goat anti-rabbit IgG (1:1000; MedChemExpress, HY-P8003), and Alexa Fluor 647-conjugated goat anti-mouse IgG (1:1000; MedChemExpress, HY-P81013). Nuclei were counterstained with DAPI (1:1000; Beyotime, C1006). Finally, sections were mounted on slides and coverslipped with antifading mounting medium. Fluorescent images were captured using a laser scanning confocal microscope (Olympus FV10).

Statistical analysis

Experimenters were blinded to treatment conditions during data collection (e.g., electrophysiological recordings) and behavioral analysis to prevent observer bias. Data are expressed as means \pm SEM. Two-tailed paired t-tests were used for electrophysiological data, one-way analysis of variance (ANOVA) for Western blot and drug microinjection data, and two-way ANOVA for the IA2BC model and Skinner box data, all with a significance level of $p < 0.05$. Tukey's test was used for post-hoc analyses when the initial p-value was significant. All data were analyzed using GraphPad Prism (version 8.0.2, San Diego, California, USA). Sample sizes were determined based on previous studies investigating LTP_{GABA} and BDNF effects, ensuring adequate power to detect significant effects. Normality tests and homogeneity test of variance were conducted prior to applying the unpaired t test, paired t test, one-way ANOVA and two-way ANOVA. The data were considered to conform to normal distribution and homogeneity of variance when the obtained p-values were no-significant.

LTP levels were determined by comparing average eIPSC amplitude 5 min before HFS to the average eIPSC amplitude during the 5 min from 20

to 25 min post-HFS. Paired-pulse ratio (PPR, 50 ms interval) and the coefficient of variation (CV) were measured from 30 eIPSCs during this 5-min period. PPR, a presynaptic parameter [52], represents the ratio of the average amplitude of 30 eIPSC2 to 30 eIPSC1 in this study. CV² of the synaptic current amplitude is negatively correlated with the release probability [53], calculated as the square of the average amplitude of 30 eIPSCs divided by their variance.

RESULTS

Chronic ethanol exposure dynamically reshapes VTA DA neuron activity in vivo

To investigate the neural basis of chronic alcohol use disorder (AUD), we first established stable chronic ethanol consumption in mice using the intermittent access two-bottle choice (IA2BC) paradigm (Fig. 1A). Over 21 days, mice exhibited escalating ethanol intake and sustained preference, while total fluid intake and body weight remained unchanged (Fig. 1B-E), confirming a valid model of chronic ethanol exposure without confounding metabolic effects.

To define the neural adaptations underlying this behavioral progression, we measured the activity of VTA DA neurons in vivo throughout the IA2BC timeline. We expressed the calcium indicator GCaMP7f specifically in VTA DA neurons of DAT-Cre mice and recorded population calcium signals via fiber photometry in freely behaving animals during 1-hour sessions on different days of ethanol exposure (days 1, 3, 7, and 21) (Fig. 1F, G).

Aligning signals to individual drinking events revealed a dramatic and specific characteristic of DA neurons responses to ethanol, but not to water (Fig. 1H-K). The population-level analysis, visualized in heatmaps sorted by magnitude, demonstrated a clear progressive action responding to ethanol exposure: initial modest activation (day 1, 3% ethanol), followed by a potentiated response (day 3, 6% ethanol), then an attenuated and unstable response phase upon first exposure to high concentration of ethanol (day 7, 20% ethanol), and finally stayed on a stabilized, hyper-reactive state after prolonged exposure (day 21, 20% ethanol) (Fig. 1L). In control group, these responses to water remained stable across all stages (Fig. 1L).

Quantitative analysis verified these dynamic changes. Both the peak amplitude ($\Delta F/F$) and area under the curve (AUC) of calcium transients evoked by ethanol licking increased significantly across the four stages (Fig. 1M, N, red). Such changes were not observed for water-licking events (Fig. 1M, N, blue). These in vivo findings suggest a failure in the normal inhibitory regulation of DA neuron activity following chronic ethanol exposure.

Chronic ethanol exposure impairs LTP_{GABA} in a presynaptic manner in VTA DA neurons

Given that synaptic plasticity, particularly long-term potentiation at GABAergic synapses (LTP_{GABA}), serves as a "brake" on DA neuron excitability in the VTA, we hypothesized that impairment of LTP_{GABA} might underlie the observed dysregulation. We applied ex vivo whole-cell recordings of eIPSCs (Fig. 2A-D) to examine the effects of chronic ethanol exposure on LTP_{GABA} in VTA DA neurons. In brain slices from ethanol-naïve mice, high-frequency stimulation (HFS) reliably induced robust LTP_{GABA} (Fig. 2E, G, H). However, HFS completely failed to induce LTP_{GABA} in slices of chronic ethanol-exposed mice (Fig. 2F, G, I), demonstrating that chronic ethanol exposure impairs this form of inhibitory synaptic plasticity. To elucidate probability that this impairment acts on presynaptic or postsynaptic site, we analyzed paired-pulse ratio (PPR) and the coefficient of variation ($1/CV^2$). In control group, HFS induced a significant decrease in PPR and an increase in $1/CV^2$, supporting a presynaptic expression mechanism of LTP_{GABA} (Fig. 2J, K, M, N; see representative raw traces in Supplementary Fig. S2). However, in ethanol-exposed mice, HFS failed to elicit these presynaptic changes (Fig. 2J, L, M, O; see representative raw

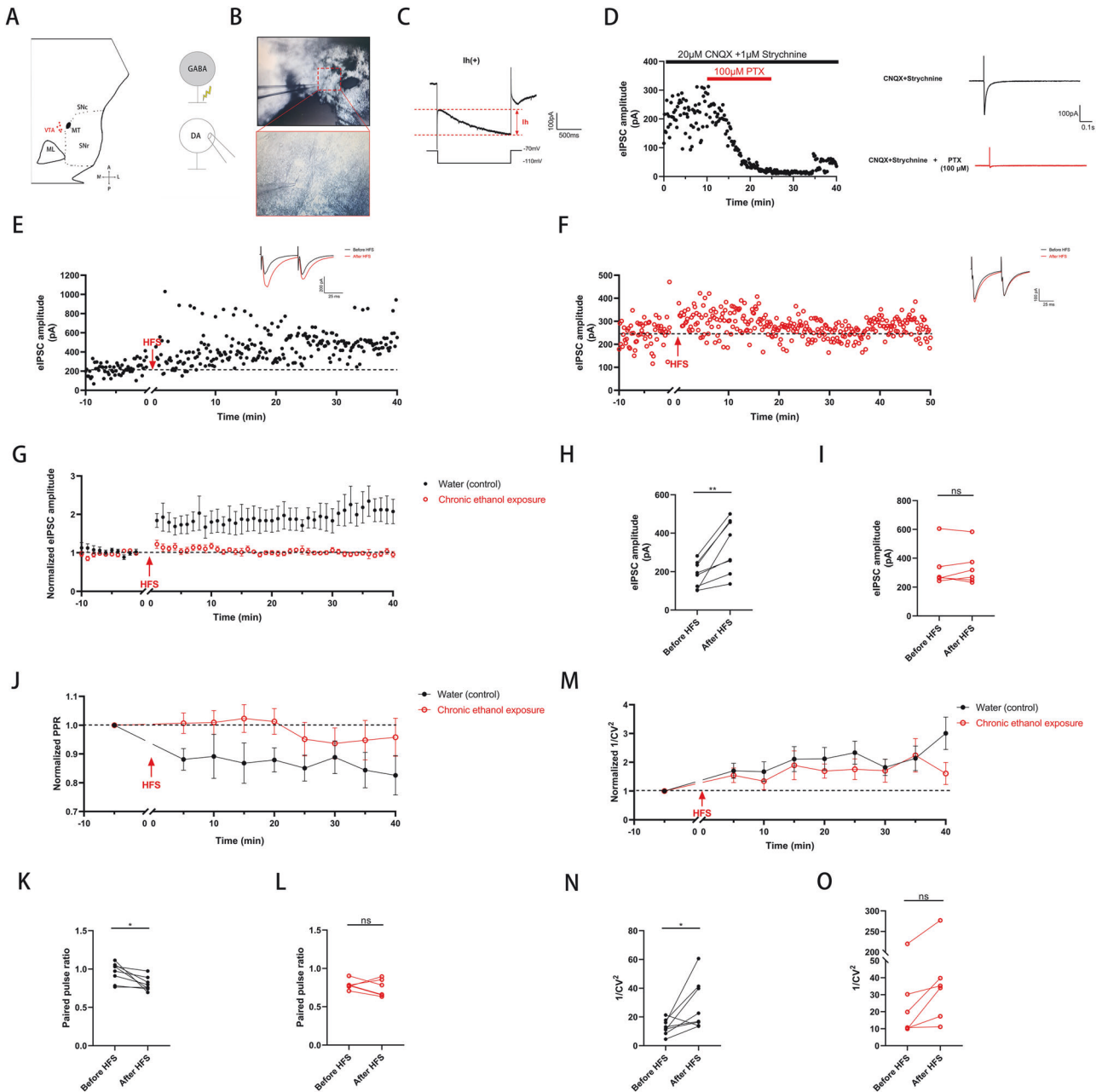


Fig. 2 Chronic Ethanol Exposure impairs LTP_{GABA} in a Presynaptic manner in VTA DA Neurons. (A) Schematic of the recording configuration in a VTA slice. The red dot indicates a recorded DA neuron, and the bipolar stimulating electrode (stim) was placed rostral to the VTA. MT, medial terminal nucleus of the accessory optic tract. (B) Representative images of the recording. Top: A VTA slice under a 10x objective. Bottom: A patched DA neuron (indicated by the pipette) under a 40x objective. (C) Identification of a putative DA neuron by a large hyperpolarization-activated current (Ih). A voltage at -110 mV elicited an Ih >100 pA. (D) Pharmacological isolation of $GABA_A$ receptor-mediated eIPSC. Bath application of $100 \mu\text{M}$ picrotoxin (PTX) blocked the evoked currents. (E) High-frequency stimulation (HFS, 100 Hz) induced LTP_{GABA} in slices from ethanol-naïve (water control) mice. Insets show average eIPSC traces before (black) and 20–25 min after HFS (red). (F) HFS failed to induce LTP_{GABA} in slices from chronic ethanol-exposed mice. Insets show average eIPSC traces before and after HFS for control (black, $n = 8$ cells/6 mice) and chronic ethanol exposed group (red, $n = 6$ cells/6 mice). Data are mean \pm SEM. (G) Time course of normalized eIPSC amplitude before and after HFS for control (black, $n = 8$ cells/6 mice) and chronic ethanol exposed group (red, $n = 6$ cells/6 mice). Data are mean \pm SEM. (H) Summary of mean eIPSC amplitude before and after HFS in control mice (Before: 183.8 ± 24.01 pA; After: 331.7 ± 48.96 pA; paired t-test, $p < 0.01$). (I) Summary of mean eIPSC amplitude before and after HFS in chronic ethanol-exposed mice (Before: 331.8 ± 56.45 pA; After: 338.3 ± 53.25 pA; paired t-test, $p > 0.05$). (J) Time course of normalized paired-pulse ratio (PPR) before and after HFS (black for water group, $n = 8$ cells/6 mice; red for chronic ethanol exposed group, $n = 6$ cells/6 mice). (K) Summary of PPR before and after HFS in control mice (Before: 0.96 ± 0.05 ; After: 0.80 ± 0.03 ; paired t-test, $p < 0.05$). (L) Summary of PPR before and after HFS in chronic ethanol-exposed mice (Before: 0.79 ± 0.03 ; After: 0.75 ± 0.05 ; paired t-test, $p > 0.05$). (M) Time course of normalized $1/CV^2$ before and after HFS (black for water group, $n = 8$ cells/6 mice; red for chronic ethanol exposed group, $n = 6$ cells/6 mice). (N) Summary of $1/CV^2$ before and after HFS in control mice (Before: 13.02 ± 1.88 ; After: 28.17 ± 6.08 ; paired t-test, $p < 0.05$). (O) Summary of $1/CV^2$ before and after HFS in chronic ethanol-exposed mice (Before: 50.18 ± 34.11 ; After: 69.08 ± 41.85 ; paired t-test, $p > 0.05$). All summary bar graphs show mean \pm SEM. * $p < 0.05$, ** $p < 0.01$, n.s., not significant.

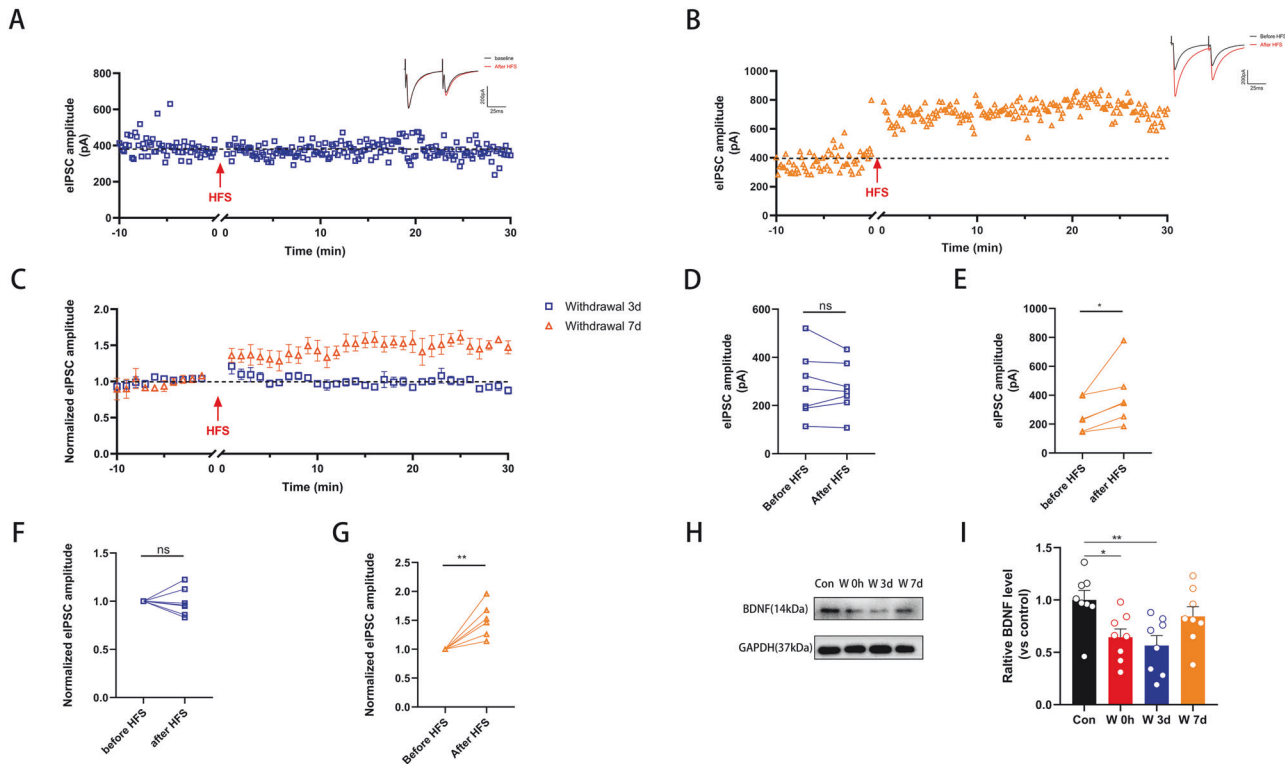


Fig. 3 Impaired LTP_{GABA} by Chronic Ethanol Exposure Recovers after 7 Days of Withdrawal. (A) A representative experiment illustrating failed HFS-induced LTP_{GABA} in a VTA DA neuron from a mouse 3 days after withdrawal from chronic ethanol exposure. Inset shows average eIPSC traces before (black) and 20–25 min after HFS (red). (B) A representative experiment showing successful HFS-induced LTP_{GABA} in a VTA DA neuron from a mouse 7 days after withdrawal. Inset as in (A). (C) Time course of averaged normalized eIPSC amplitudes before and after HFS for the 3-day (blue, $n = 7$ cells/5 mice) and 7-day (orange, $n = 6$ cells/6 mice) withdrawal groups. Data are mean \pm SEM. (D) Summary of mean eIPSC amplitude before and after HFS in the 3-day withdrawal group (Before: 285.2 ± 51.93 pA; After: 272.5 ± 40.31 pA; paired t-test, $p > 0.05$). (E) Summary of mean eIPSC amplitude before and after HFS in the 7-day withdrawal group (Before: 260.0 ± 46.73 pA; After: 394.1 ± 85.8 pA; paired t-test, $p < 0.05$). (F) Summary of normalized eIPSC amplitude change for the 3-day withdrawal group ($99.02 \pm 5.30\%$; $p > 0.05$ vs. baseline). (G) Summary of normalized eIPSC amplitude change for the 7-day withdrawal group ($150.4 \pm 12.01\%$; $p < 0.01$ vs. baseline). (H) Representative western blot images showing BDNF protein levels in the VTA from control (Con) and ethanol-exposed mice at 0 hours (W 0 h), 3 days (W 3 d), and 7 days (W 7 d) after withdrawal. GAPDH served as a loading control. (I) Quantification of BDNF protein levels normalized to GAPDH. One-way ANOVA revealed a significant effect ($F(3,28) = 4.78$, $p < 0.01$). Post hoc Tukey's test: Con vs. W 0 h: $p < 0.05$; Con vs. W 3 d: $p < 0.01$. $n = 8$ mice per group. Data are mean \pm SEM. * $p < 0.05$, ** $p < 0.01$, n.s., not significant.

traces in Supplementary Fig. S2). These results indicate that chronic ethanol exposure disrupts LTP_{GABA} by specifically reducing the presynaptic GABA release probability.

Notably, chronic ethanol exposure also altered basal GABAergic transmission, as evidenced by increased baseline eIPSC amplitude and decreased paired-pulse ratio (PPR) in ethanol exposure mice (Fig. 2H, I, K, L), suggesting an elevated presynaptic release probability in duce by chronic ethanol exposure. To ensure that these baseline changes did not confound the assessment of synaptic plasticity, we performed an analysis of covariance (ANCOVA). The lack of a significant group \times baseline interaction ($F(1,12) = 0.38$, $p = 0.55$) and the absence of a correlation between baseline amplitude and the magnitude of LTP ($F(1,12) = 0.63$, $p = 0.43$) confirm that the blockade of HFS-induced LTP_{GABA} reflects an impairment of synaptic plasticity surely, independent of pre-existing alterations in basal synaptic strength.

Impaired LTP_{GABA} by chronic ethanol exposure recovers after 7 days of withdrawal

We next asked whether the impairment of LTP_{GABA} induced by chronic ethanol exposure was reversible after cessation of drinking. Electrophysiological recordings on VTA DA neurons revealed that LTP_{GABA} remained absent 3 days after withdrawal (Fig. 3A, C, D, F). However, 7 days post-withdrawal, HFS successfully induced LTP_{GABA} with a magnitude comparable to

that in ethanol-naïve mice (Fig. 3B, C, E, G), indicating a full recovery of this inhibitory synaptic plasticity. Given its closely involving action on synaptic plasticity, the temporal profile of this recovery prompted us to examine the expression levels of BDNF in VTA on different time points. We measured BDNF expression in the VTA across the above withdrawal time points. Western blot analysis showed that BDNF protein levels, significantly decreased after chronic exposure till 3 days after withdrawal, and returned to baseline level 7 days after withdrawal (Fig. 3H, I), indicating a close temporal correlation between the restoration of inhibitory synaptic plasticity and BDNF expression.

BDNF-TrkB signaling is necessary and sufficient for LTP_{GABA} induction in VTA DA neurons

Having established the temporal correlation between BDNF expression and LTP_{GABA} recovery, we next sought to determine whether BDNF-TrkB signaling is mechanistically required for LTP_{GABA}. We first assessed the effect of blocking TrkB receptors using the selective antagonist K252a in VTA slices from ethanol-naïve mice. Bath application of K252a prior to HFS completely prevented the induction of LTP_{GABA} (Fig. 4A–D). In contrast, when K252a was applied after HFS, it did not affect the maintenance of already established LTP_{GABA} (Fig. 4E–H). These results indicate that TrkB activation is specifically required for the induction, but not the maintenance, of LTP_{GABA}. We then tested whether BDNF itself

Fig. 4 BDNF induces LTP_{GABA} via TrkB activation in VTA DA neurons. (A) A representative experiment showing that bath application of the TrkB antagonist K252a (200 nM) prior to HFS blocks LTP_{GABA} induction. Inset shows average eIPSC traces before (black) and 20–25 min after HFS (red). (B) Time course of normalized eIPSC amplitude before and after K252a application and HFS (n = 7 cells/6 mice). (C) Summary of mean eIPSC amplitude before and after HFS in the presence of pre-application K252a (Before: 224.5 ± 68.11 pA; After: 214.9 ± 70.01 pA; paired t-test, p > 0.05). (D) Summary of normalized eIPSC amplitude change with pre-application K252a (93.27 ± 7.93%; p > 0.05 vs. baseline). (E) A representative experiment showing that bath application of K252a (200 nM) after HFS does not affect LTP_{GABA} maintenance. (F) Time course of normalized eIPSC amplitude before and after HFS followed by K252a application (n = 6 cells/6 mice). (G) Summary of mean eIPSC amplitude before and after HFS followed by K252a application (Before: 241.3 ± 48.3 pA; After: 339.0 ± 52.96 pA; paired t-test, p < 0.01). (H) Summary of normalized eIPSC amplitude change with post-HFS K252a application (148.5 ± 11.0%; p < 0.01 vs. baseline). (I) A representative experiment showing that bath application of exogenous BDNF (20 ng/mL) induces LTP_{GABA} in the absence of HFS. (J) Time course of normalized eIPSC amplitude before and after BDNF application (n = 9 cells/8 mice). (K) Summary of mean eIPSC amplitude before and after BDNF application (Before: 228.6 ± 21.22 pA; After: 486.0 ± 95.42 pA; paired t-test, p < 0.05). (L) Summary of normalized eIPSC amplitude change induced by BDNF (201.9 ± 24.79%; p < 0.01 vs. baseline). (M) A representative experiment showing that BDNF-induced LTP_{GABA} is blocked when K252a (200 nM) is present throughout the recording. (N) Time course of normalized eIPSC amplitude before and after BDNF application in the continuous presence of K252a (n = 6 cells/6 mice). (O) Summary of mean eIPSC amplitude before and after BDNF + HFS in the presence of K252a (Before: 176.8 ± 27.93 pA; After: 166.0 ± 23.51 pA; paired t-test, p > 0.05). (P) Summary of normalized eIPSC amplitude change with BDNF + HFS in the presence of K252a (96.16 ± 4.49%; p > 0.05 vs. baseline). All summary data are presented as mean ± SEM. *p < 0.05, **p < 0.01, n.s., not significant.

Thus, combining pharmacological blockade and region-specific genetic knockdown, we conclusively demonstrate that BDNF signaling through its receptor TrkB in the VTA is indispensable for the induction of LTP_{GABA} at GABAergic synapses on DA neurons.

BDNF attenuates ethanol-seeking behavior by restoring LTP_{GABA} and dynamics of DA neuron activity

Having established the necessity of BDNF-TrkB signaling for LTP_{GABA}, we next investigated its functional relevance in ethanol-related behaviors and the underlying neural dynamics in vivo. We first trained mice to self-administer 10% ethanol in an operant conditioning chamber, where active lever pressing was paired with a discrete cue light (Fig. 6A). After 19 days of fixed-ratio training, mice developed stable cue-induced ethanol seeking, with significantly more presses on the active lever than the inactive lever (Fig. 6B and Supplementary Fig. S3A). In subsequent extinction training mice, active lever presses without delivering ethanol or cues, significantly decreased (Supplementary Fig. S3B).

To assess the effect of BDNF on the motivation of ethanol seeking, we microinjected BDNF or vehicle directly into the VTA of ethanol self-administering mice (Fig. 6C). BDNF infusion significantly reduced the breakpoint in a progressive ratio paradigm, indicating a lower motivation for ethanol (Fig. 6D). This effect was blocked by co-infusion of the TrkB antagonist K252a with BDNF, confirming effects of BDNF depending on TrkB activation. Consistent with this attenuated motivation, BDNF treatment also decreased the total amount of ethanol consumed during the test session, which effect was blocked by co-infusion of K252a (Supplementary Fig. S3C). Infusion of K252a into VTA alone had no effect on either measurement (Fig. 6D, Supplementary Fig. S3C).

We then sought to determine whether this reduction in operant seeking was associated with status of the hyperactive DA neuron activities characterized in chronic ethanol-exposed mice (Fig. 1), and whether this action involved enhanced GABAergic signaling. We performed in vivo fiber photometry recordings in VTA DA neurons of DAT-cre mice undergoing the IA2BC paradigm training under conditions of intra-VTA microinjection of vehicle, BDNF, the GABA_A receptor agonist muscimol, BDNF+K252a, or BDNF+Gabazine (a GABA_A receptor antagonist) respectively (Fig. 6E).

BDNF treatment significantly attenuated the peak of calcium transients evoked by ethanol licking (Fig. 6F, G, L). Crucially, muscimol mimicked the effect of BDNF, similarly reducing ethanol-evoked responses, suggesting that enhancing GABA_A receptor activity is sufficient to restore dynamics DA neuron activity (Fig. 6H, L). Co-administration of K252a or gabazine completely blocked BDNF's effect (Fig. 6I, J, L). In control group, none of the drug treatments altered DA neuron responses to

water licking (Fig. 6F–J, L, M). Population heatmaps and analysis of the area under the curve (AUC) further illustrated the specific restoration against ethanol-evoked responses (Fig. 6K, M).

Finally, to test if this rapid restoration of dynamics DA neuron activity in vivo is related to synaptic repairment, we returned to ex vivo slice physiology. In VTA slices from chronic ethanol-exposed mice that had undergone the IA2BC paradigm, bath application of BDNF successfully rescued HFS-induced LTP_{GABA}, which was absent otherwise (Fig. 6N–Q).

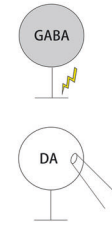
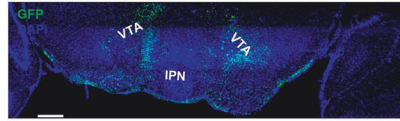
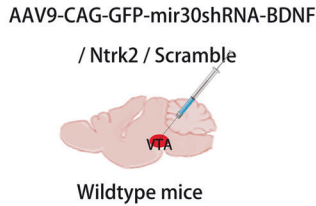
Together, these results demonstrate that enhancing BDNF signaling in the VTA attenuates the ethanol motivation by restoring GABAergic inhibitory regulation. This restoration may occur at two levels: BDNF restores the hyperactive in vivo acting patterns of DA neurons during consumption (an effect mimicked by GABA_A receptor activation and blocked by GABA_A or TrkB antagonist), and concurrently repairs the impaired LTP_{GABA} that is essential for maintaining inhibitory tone.

DISCUSSION

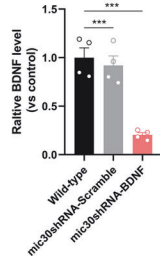
In this study, we found that chronic ethanol exposure impaired HFS-induced LTP_{GABA} in the VTA via reducing presynaptic GABA release. This plasticity deficit recovers after 7 days of withdrawal, paralleling the restoration of BDNF protein levels in the VTA. Using both pharmacological and region-specific genetic knockdown, we found that BDNF signaling through TrkB is necessary and sufficient for LTP_{GABA} induction. Crucially, exogenous BDNF application rescues the impaired LTP_{GABA} in slices from ethanol-exposed mice. In vivo, intra-VTA BDNF microinjection rapidly restores the hyperactive calcium responses in DA neurons during ethanol consumption, a key finding revealed by our fiber photometry recordings, and significantly attenuates cue-driven ethanol-seeking behavior. These behavioral and in vivo neural dynamics depend on TrkB activation, and were mimicked by enhancing GABA_A receptor signaling.

Drug addiction is widely viewed as a maladaptive learned behavior [54], in which dopamine dysregulation contributes to disrupted motivation and habitual drug pursuit [55]. Changes in synaptic efficacy, such as LTD and LTP, are likely fundamental mechanisms underlying learning, memory, and addiction [2, 5]. LTP at inhibitory synapses onto VTA DA neurons has been proposed to act as a “brake” on dopaminergic excitability [13, 14]. Our findings reveal that chronic ethanol exposure inhibits LTP_{GABA} by reducing presynaptic GABA release, extending our earlier findings regarding acute ethanol exposure [12]. Interestingly, we also observed that chronic ethanol exposure altered basal GABAergic transmission, increasing the baseline eIPSC amplitude and decreasing the paired-pulse ratio indicating an elevated

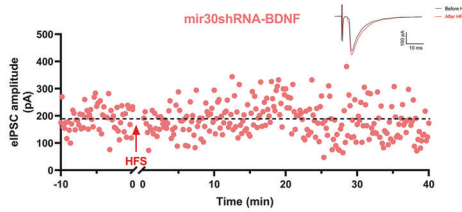
A



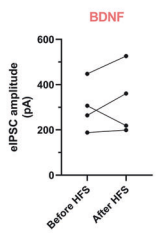
B



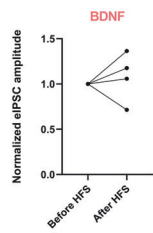
C



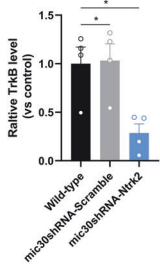
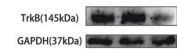
D



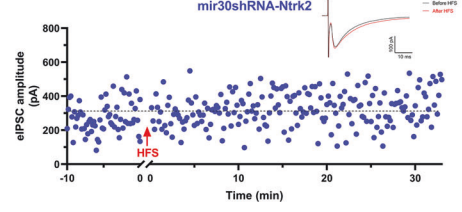
E



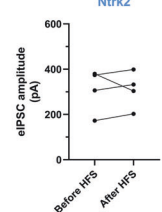
F



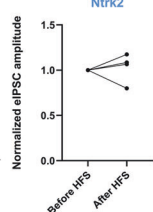
G



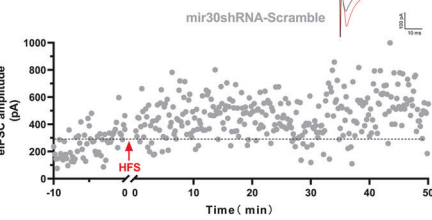
H



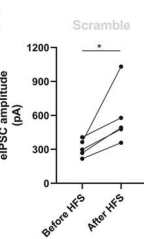
I



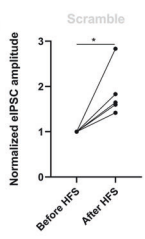
J



K



L



M

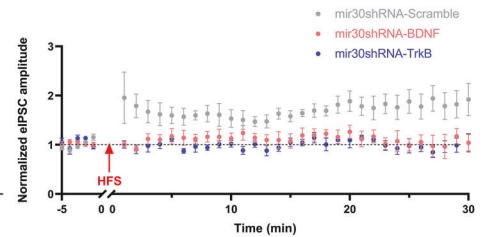
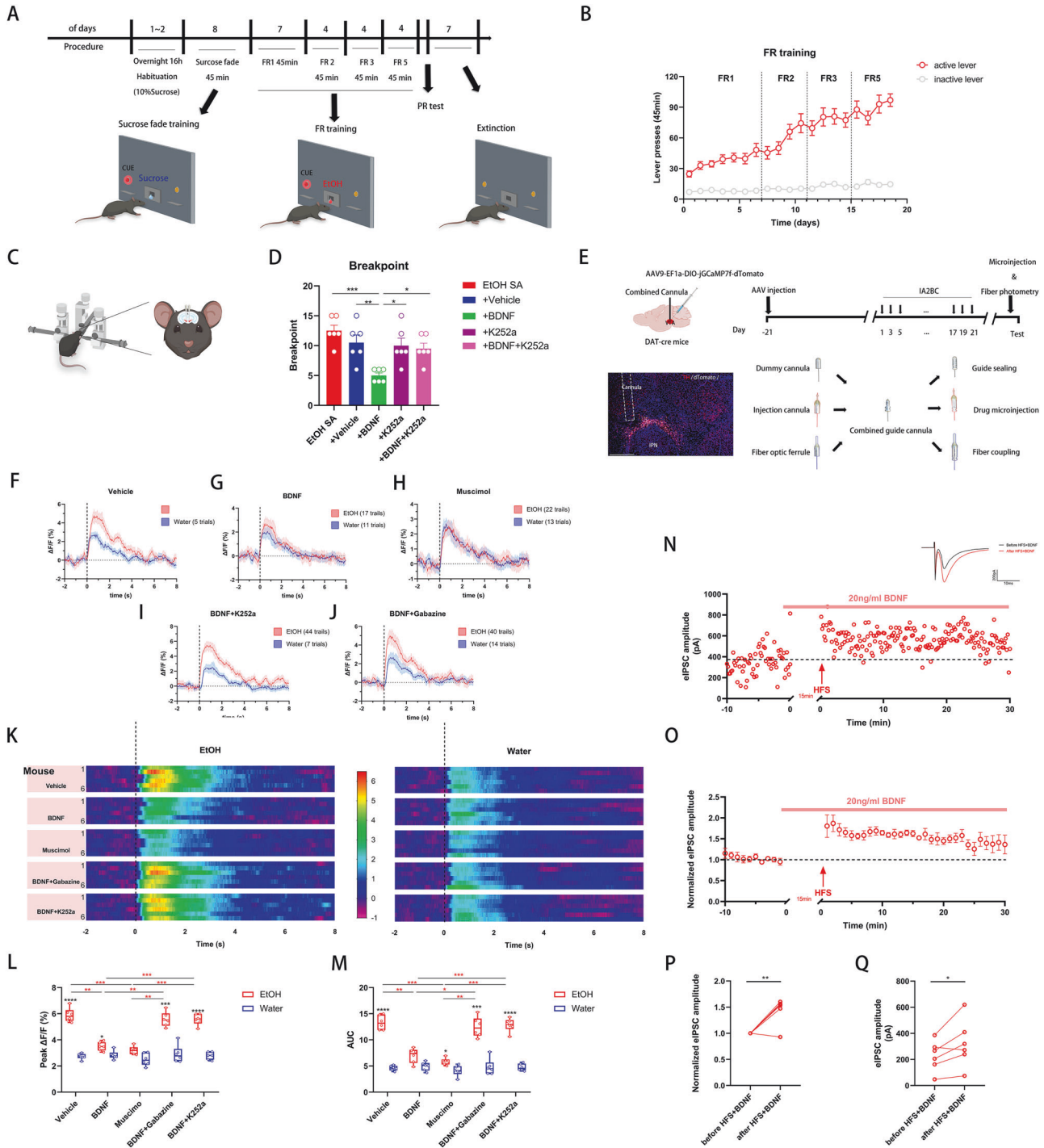


Fig. 5 BDNF-TrkB Signaling is Indispensable for LTP_{GABA} Induction. (A) Schematic of the experimental strategy (left). AAV9 vectors expressing mir30shRNA targeting BDNF, TrkB (Ntrk2), or a scrambled control sequence under the CAG promoter were bilaterally injected into the VTA of wild-type mice. Middle: Coronal VTA section showing GFP expression (green) and DAPI (blue) three weeks after AAV injection. Scale bar, 100 μm. Right: Schematic of the ex vivo recording configuration for measuring eIPSCs. (B) Validation of BDNF knockdown in the VTA by western blot. Left: Representative blot for BDNF and GAPDH. Right: Quantification shows BDNF protein was reduced to 20.35 ± 2.36% of the level in scramble-injected controls (n = 4 mice per group; unpaired t-test, p < 0.05). (C) A representative experiment showing that HFS fails to induce LTP_{GABA} in a VTA DA neuron from a mouse with VTA-specific BDNF knockdown. (D) Summary of mean eIPSC amplitude before and after HFS in BDNF knockdown mice (Before: 301.7 ± 54.53 pA; After: 326.2 ± 75.78 pA; paired t-test, p > 0.05). (E) Summary of normalized eIPSC amplitude change in BDNF knockdown mice (107.8 ± 13.68%; p > 0.05 vs. baseline; n = 4 cells/4 mice). (F) Validation of TrkB knockdown by western blot. Left: Representative blot for TrkB and GAPDH. Right: Quantification shows TrkB protein was reduced to 28.54 ± 9.58% of control levels (n = 4 mice per group; unpaired t-test, p < 0.05). (G) A representative experiment showing that HFS fails to induce LTP_{GABA} in a VTA DA neuron from a mouse with VTA-specific TrkB knockdown. (H) Summary of mean eIPSC amplitude before and after HFS in TrkB knockdown mice (Before: 308.2 ± 48.23 pA; After: 309.3 ± 40.77 pA; paired t-test, p > 0.05). (I) Summary of normalized eIPSC amplitude change in TrkB knockdown mice (103.1 ± 8.09%; p > 0.05 vs. baseline; n = 4 cells/4 mice). (J) A representative experiment showing that HFS successfully induces LTP_{GABA} in a VTA DA neuron from a mouse injected with the control (scramble) AAV. (K) Summary of mean eIPSC amplitude before and after HFS in scramble control mice (Before: 311.3 ± 33.73 pA; After: 587.5 ± 116.4 pA; paired t-test, p < 0.05). (L) Summary of normalized eIPSC amplitude change in scramble control mice (186.7 ± 25.06%; p < 0.05 vs. baseline; n = 5 cells/4 mice). (M) Time course of averaged normalized eIPSC amplitudes for all three groups before and after HFS, illustrating the specific blockade of LTP_{GABA} induction in BDNF (red) and TrkB (green) knockdown groups compared to the scramble control (gray). Data are mean ± SEM. *p < 0.05.



presynaptic release probability in chronic ethanol exposure mice. To confirm that these baseline differences did not artifactually influence our assessment of plasticity, we performed an analysis of covariance (ANCOVA). The non-significant group \times baseline interaction and the absence of a correlation between baseline amplitude and LTP magnitude collectively demonstrate that the ethanol-induced suppression of LTP_{GABA} represents a genuine deficit in synaptic plasticity, rather than a confusing measurement. It is important to note that mechanisms of HFS-induced inhibitory synaptic LTP vary significantly across brain regions. In visual cortex, LTP_{GABA} induction relies on the activation of postsynaptic GABA_B receptors that enhance IP3 synthesis

triggered by monoamines, leading to the release of intracellular Ca²⁺ [56]; whereas in the VTA, it involves a retrograde signaling pathway dependent on nitric oxide-cyclic guanosine monophosphate-protein kinase G (NO-cGMP-PKG pathway) [13, 57]. We propose three non-mutually exclusive mechanisms through which chronic ethanol may impair this plasticity: (1) Epigenetic modifications of μ -opioid receptor (MOR) mRNA via m⁶A methylation, as reported after chronic intermittent ethanol [58], could disrupt NO-cGMP-PKG signaling downstream of opioid receptors; (2) Bidirectional crosstalk between BDNF-TrkB signaling and NO pathways: where BDNF-TrkB signaling enhances neuronal nitric oxide synthase (nNOS)-dependent NO synthesis [59] and

Fig. 6 BDNF Attenuates Ethanol-Seeking Behavior by Restoring GABAergic Inhibition and dynamics of DA Neuron Activity. (A) Timeline of the operant ethanol self-administration (SA) experiment and drug testing. Mice were trained to self-administer 10% ethanol, underwent extinction, and were then tested following intra-VTA drug microinjection. (B) The number of active and inactive lever presses per session across fixed-ratio (FR) training days, showing stable acquisition of operant responding ($n = 12$ mice). See Supplementary Fig. S3A for a representative raster plot. (C) Schematic of intra-VTA drug microinjection via a guide cannula. (D) The breakpoint in a progressive ratio (PR) test for mice treated with Vehicle, BDNF, K252a, or BDNF+K252a. One-way ANOVA: $F(4, 15) = 7.403$, $p < 0.01$. *Post hoc* Tukey's test: EtOH SA vs. BDNF: 12.50 ± 0.9220 vs. 5.00 ± 0.4472 , $p < 0.0001$; Vehicle vs. BDNF: 10.50 ± 1.285 vs. 5.00 ± 0.4472 , $p < 0.01$; BDNF vs. K252a: 5.00 ± 0.4472 vs. 10.00 ± 1.265 , $p < 0.05$; BDNF vs. BDNF+K252a: 5.00 ± 0.4472 vs. 9.50 ± 0.922 , $p < 0.05$. $n = 6$ mice per group. (E) In vivo recording strategy. Top left: Schematic for jGCaMP7f expression. Bottom left: Coronal VTA section showing TH+ neurons (red), jGCaMP7f reporter (gray), and DAPI (blue). Scale bar, 100 μm . Top right: Timeline of the IA2BC and photometry recording experiment. Bottom right: Design of the custom combined cannula for guide sealing, drug microinjection, and fiber coupling. (F–J) Representative average calcium transients ($\Delta F/F$) aligned to licking onset (dashed line at 0 s) for ethanol (red) and water (blue) from a single mouse per group following intra-VTA treatment with Vehicle (F), BDNF (G), Muscimol (H), BDNF+Gabazine (I), or BDNF+K252a (J). Traces are mean \pm SEM of all trials from one representative animal. (K) Population heatmaps of $\Delta F/F$ responses (aligned to lick onset, dashed line). Left: Ethanol licking events. Right: Water licking events. Each row represents the average response of one mouse ($n = 6$ mice per group). (L) Quantification of peak $\Delta F/F$ for ethanol (red) and water (blue) events across drug treatment groups. Two-way ANOVA revealed significant main effects of Drug ($F(4, 40) = 25.95$, $p < 0.0001$) and Fluid (Ethanol vs. Water) ($F(1, 10) = 227.1$, $p < 0.0001$), with a significant interaction ($F(4, 40) = 27.61$, $p < 0.0001$). *Post hoc* comparisons for ethanol responses (Tukey's test): Vehicle ($5.89 \pm 0.22\%$) vs. BDNF ($3.50 \pm 0.14\%$), $p = 0.0013$; Vehicle vs. Muscimol ($3.20 \pm 0.13\%$), $p = 0.0009$; BDNF vs. BDNF+Gabazine ($5.57 \pm 0.23\%$), $p = 0.0057$; BDNF vs. BDNF+K252a ($5.57 \pm 0.17\%$), $p = 0.0004$; Muscimol vs. BDNF+Gabazine, $p = 0.0040$; Muscimol vs. BDNF+K252a, $p = 0.0002$. Water responses did not differ between groups. Within-group comparisons (Bonferroni's test): Vehicle (Water: $2.72 \pm 0.09\%$), $p < 0.0001$; BDNF (Water: $2.83 \pm 0.13\%$), $p = 0.0279$; BDNF+Gabazine (Water: $2.91 \pm 0.27\%$), $p = 0.0001$; BDNF+K252a (Water: $2.79 \pm 0.12\%$), $p < 0.0001$. (M) Quantification of area under the curve (AUC, %·s) for ethanol (red) and water (blue) events. Two-way ANOVA revealed significant main effects of Drug ($F(4, 40) = 25.63$, $p < 0.0001$) and Fluid ($F(1, 10) = 302.1$, $p < 0.0001$), with a significant interaction ($F(4, 40) = 28.49$, $p < 0.0001$). *Post hoc* comparisons for ethanol responses (Tukey's test): Vehicle ($13.33 \pm 0.56\%$ ·s) vs. BDNF ($6.99 \pm 0.57\%$ ·s), $p = 0.0049$; Vehicle vs. Muscimol ($5.88 \pm 0.27\%$ ·s), $p = 0.0010$; BDNF vs. BDNF+Gabazine ($12.45 \pm 0.78\%$ ·s), $p = 0.0177$; BDNF vs. BDNF+K252a ($12.84 \pm 0.52\%$ ·s), $p = 0.0004$; Muscimol vs. BDNF+Gabazine, $p = 0.0063$; Muscimol vs. BDNF+K252a, $p = 0.0001$. Water responses did not differ between groups. Within-group comparisons (Bonferroni's test): Vehicle (Water: $4.60 \pm 0.20\%$ ·s), $p < 0.0001$; Muscimol (Water: $4.11 \pm 0.41\%$ ·s), $p = 0.0296$; BDNF+Gabazine (Water: $4.79 \pm 0.63\%$ ·s), $p = 0.0001$; BDNF+K252a (Water: $4.75 \pm 0.28\%$ ·s), $p < 0.0001$. (N) A representative experiment showing that bath application of BDNF (20 ng/mL) restores HFS-induced LTP_{GABA} in a VTA slice from a chronic ethanol-exposed mouse. Insets show average eIPSC traces before (black) and 20–25 min after HFS (red). (O) Time course of normalized eIPSC amplitude before and after HFS with BDNF application ($n = 6$ cells/6 mice). (P) Summary of mean eIPSC amplitude before and after HFS with BDNF (Before: 227.1 ± 47.72 pA; After: 322.6 ± 74.64 pA; paired t-test, $p < 0.05$). (Q) Summary of normalized eIPSC amplitude change with BDNF ($144.3 \pm 10.43\%$; $p < 0.01$ vs. baseline). All summary data are mean \pm SEM. * $p < 0.05$, ** $p < 0.01$, *** $p < 0.001$, **** $p < 0.0001$.

NO-mediated nitration reciprocally modulates TrkB function [60] may be disrupted under low levels of BDNF conditions, impairing postsynaptic NMDAR (GluN2A/2B-containing)-dependent LTP_{GABA} induction; (3) Chronic ethanol exposure reduces synaptic proteins (e.g., PSD-95) and dendritic spine density [61], which could compromise GABAergic synaptic integrity.

Intriguingly, the presynaptic impairment of LTP_{GABA} points to a potential role of BDNF in directly modulating vesicular release machinery. Beyond its classic postsynaptic actions, BDNF-TrkB activation can lead to the opening of transient receptor potential canonical 3 (TRPC3) channels on presynaptic terminals, triggering Ca^{2+} influx that facilitates neurotransmitter release [62]. We hypothesize that the loss of this BDNF-dependent presynaptic Ca^{2+} signaling may contribute to the failure to enhance GABA release following HFS in the ethanol-exposed VTA. Future studies employing presynaptic Ca^{2+} imaging and TRPC3 manipulation may test this model directly, such as synaptophysin-pHluorin (e.g., sypHy) for monitoring vesicle fusion and genetically encoded calcium indicators for presynaptic Ca^{2+} dynamics, to dissect the precise sequence of events at the presynaptic terminal [63]. While the pharmacological TrkB antagonist K252a is a valuable tool, its potential off-target effects on other kinases necessitate cautious interpretation. Our findings are strengthened by the congruent results from VTA-specific genetic knockdown of BDNF or TrkB (Ntrk2), which recapitulated the blockade of LTP_{GABA} without affecting baseline transmission. This genetic approach provides compelling causal evidence for the specific requirement of BDNF-TrkB signaling in this form of plasticity.

Many neuroadaptations induced by chronic ethanol are reversible after withdrawal. For instance, somatic withdrawal symptoms and intracranial self-stimulation thresholds peak within hours and return to baseline within days [25, 64]. Synaptic plasticity also shows recovery; paired-pulse facilitation and LTP in the hippocampus are restored several days after ethanol withdrawal [65]. Our data demonstrated that both LTP_{GABA} and BDNF levels in the VTA recover after 7 days of abstinence. The

mechanisms underlying BDNF recovery may involve the reversal of ethanol-induced epigenetic silencing at BDNF promoters [66, 67] and the resolution of neuroinflammation, allowing glial cells to resume normal BDNF secretion [68–70]. Notably, astrocyte-derived BDNF has been shown to regulate late-phase synaptic plasticity [70], suggesting that glial contributions may be particularly important for the slow, restorative phase of inhibitory tone during prolonged withdrawal.

The role of BDNF in drug-seeking behavior is complex and region-specific. While intra-NAc BDNF enhances cocaine-seeking [26] and intra-PFC BDNF suppresses it [27], our results demonstrate that intra-VTA BDNF attenuates ethanol-seeking. This discrepancy likely reflects the distinct primary synaptic targets of different drugs; cocaine predominantly affects glutamatergic transmission [71], whereas chronic ethanol, as shown here, robustly impairs GABAergic plasticity in the VTA. The reduction in ethanol-seeking motivation after treatment of BDNF is likely mediated through its role in restoration of LTP_{GABA}, thereby inhibits activities of hyperactive DA neurons. This is consistent with studies showing that chemogenetic inhibition of VTA DA neurons reduces cue-induced alcohol-seeking [72]. Conversely, the induction of LTP at excitatory synapses within other reward-related circuits, such as the corticostriatal pathway, has been shown to enhance alcohol-seeking behavior [73].

From a translational perspective, our findings highlight BDNF-TrkB signaling in the VTA as a promising target for AUD intervention. 7,8-dihydroxyflavone (7,8-DHF), a small-molecule TrkB agonists, offers a particularly viable pharmacologic strategy. 7,8-DHF crosses the blood-brain barrier, mimics the neurotrophic effects of BDNF in brain, and our prior work has demonstrated its efficacy in reducing ethanol intake and withdrawal symptoms in rodent models [25]. Beyond pharmacological approaches, our results suggest that interventions capable of enhancing inhibitory tone within the VTA may hold therapeutic value. In this regard, non-invasive brain stimulation techniques, such as transcranial magnetic stimulation (TMS), which can modulate cortical

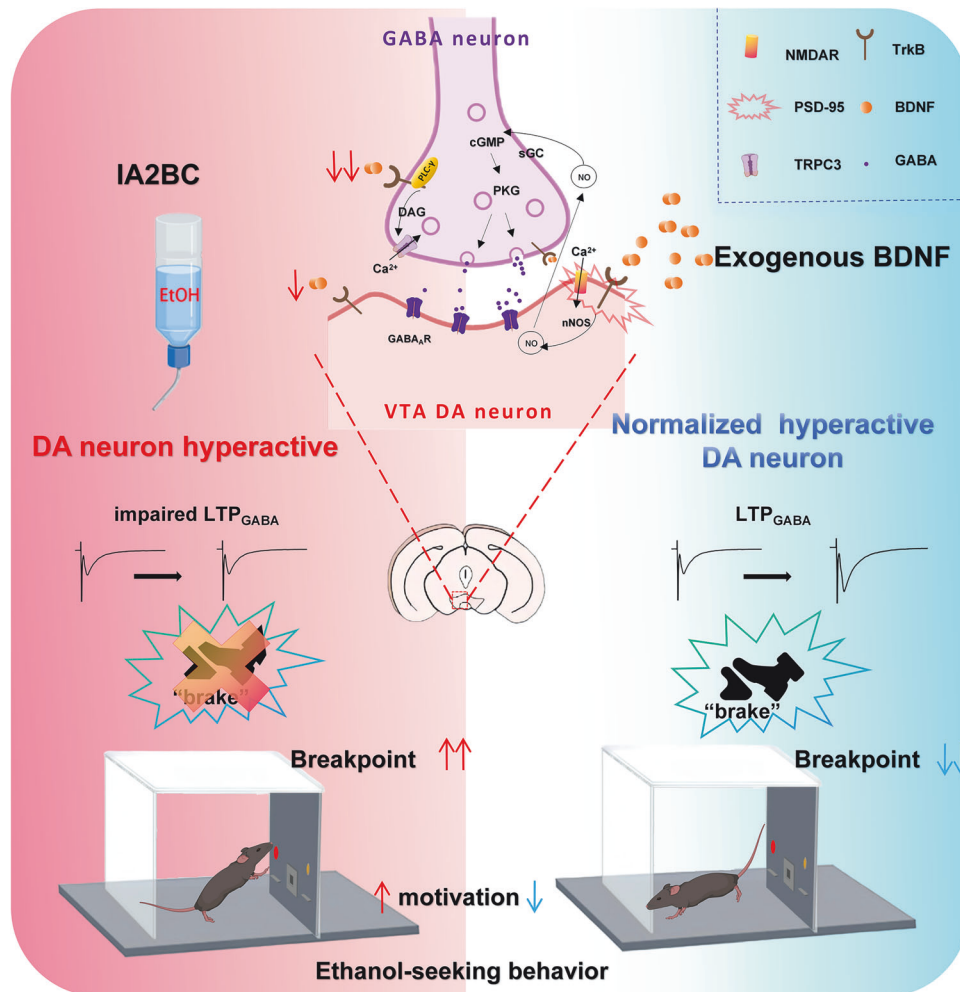


Fig. 7 BDNF Restores Ethanol-Impaired GABAergic Synaptic Plasticity and Reduces Effortful Reward-Seeking Behavior. Schematic summary of the study's key findings and proposed mechanism. (Left panel, Chronic Ethanol Exposure) In the intermittent access two-bottle choice (IA2BC) paradigm, chronic ethanol consumption decreases BDNF levels (red downward arrow) in the ventral tegmental area (VTA). This leads to impaired long-term potentiation of GABAergic synapses onto VTA DA neurons (LTP_{GABA} ; represented by unchanged eIPSC traces), which fails to provide a functional "brake" (red X over brake icon) on DA neuron activity. Consequently, DA neurons become hyperactive, contributing to increased motivation for ethanol, as evidenced by a higher breakpoint in an operant progressive ratio task (red upward arrow). The inset shows a coronal mouse brain section highlighting the VTA (red dashed box). **(Right panel, Exogenous BDNF Intervention)** Microinjection of exogenous BDNF into the VTA restores BDNF-TrkB signaling. This normalizes DA neuron hyperactivity and rescues LTP_{GABA} (represented by potentiated eIPSC traces), thereby re-engaging the inhibitory "brake". At the behavioral level, this synaptic repair translates to a significant reduction in the motivation to work for ethanol, indicated by a lower breakpoint (blue downward arrow). **(Central panel, Proposed Synaptic Mechanism)** A detailed view of a GABAergic synapse in the VTA illustrates the proposed molecular pathways. BDNF binding to postsynaptic TrkB receptors may enhance NMDAR function within the PSD-95 scaffold, leading to calcium influx, activation of neuronal nitric oxide synthase (nNOS), and production of nitric oxide (NO). NO acts as a retrograde messenger, diffusing to the presynaptic terminal to activate the sGC-cGMP-PKG pathway, ultimately promoting GABA release. Additionally, BDNF binding to presynaptic TrkB receptors may activate phospholipase C_{γ} (PLC_{γ}), leading to diacylglycerol (DAG)-mediated activation of transient receptor potential canonical 3 (TRPC3) channels, causing calcium influx that facilitates GABA vesicle release. Together, these actions converge to restore synaptic strength at inhibitory synapses.

excitability and influence subcortical circuits including the mesolimbic pathway, represent a clinically established tool worthy of future investigation. Such strategies, which aim to rebalance reward circuit activity, may be strategically deployed during the high-risk period of early abstinence. Together, these avenues, from readily testable pharmacotherapies to neuromodulation, translate our mechanistic insight into tangible therapeutic possibilities.

Therefore, we propose a unified model in which the loss and restoration of BDNF-TrkB signaling in the VTA constitute a pivotal switch governing GABAergic synaptic plasticity, DA neuron activity dynamics, and maladaptive ethanol-seeking behavior (Fig. 7). This schematic integrates our key experimental findings across scales, depicting the pathological state induced by chronic ethanol

exposure (left panel) and the restorative effects of exogenous BDNF (right panel), alongside a detailed hypothesis of the underlying pre- and postsynaptic molecular interactions (central panel). Future studies may validate the specific molecular pathways proposed in this model and to explore their translational potential.

Several limitations of this study warrant consideration. While we identified DA neurons using established electrophysiological criteria (large $I_h > 100$ pA and soma size), morphological and I_h -based identification alone is not infallible. We focused recordings in the lateral VTA where the correlation between I_h and tyrosine hydroxylase expression is high to maximize accuracy [45, 74]. The exclusive use of male mice, while reducing hormonal variability, precludes understanding of sex differences in BDNF-TrkB

modulation of LTP_{GABA} and ethanol seeking, a direction for future research because of interactions between estrogen, BDNF, and addiction vulnerability [31, 32, 75, 76]. Future studies should include females to assess sex differences in BDNF-TrkB modulation of LTP_{GABA} and ethanol-seeking behavior. Finally, GABAergic inputs to the VTA are heterogeneous, originating from local interneurons, the nucleus accumbens, and brainstem nuclei, each with potentially distinct plasticity mechanisms [42, 44, 77]. Our stimulation electrode placement may activate a mix of these afferents. Future studies using pathway-specific optogenetic stimulation, combined with in vivo LTP_{GABA} induction, will be essential to determine whether specific GABAergic circuits are preferentially impaired by ethanol and/or rescued by BDNF, and whether their rescue is sufficient to modulate the VTA-NAc DA projection during reward-seeking behaviors [78–80].

In conclusion, our results suggest that chronic ethanol exposure disrupts inhibitory synaptic plasticity in the VTA by suppressing BDNF-TrkB signaling, leading to hyperactive DA neuron activities and enhanced alcohol motivation. Restoring this pathway, either pharmacologically or genetically, rescues GABAergic potentiation, restores DA neuron dynamics, and reduces ethanol-seeking behavior. These findings establish BDNF-TrkB signaling as a critical mediator of synaptic and behavioral adaptations in AUD and reveal promising therapeutic means for AUD.

REFERENCES

- Carvalho AF, Heilig M, Perez A, Probst C, Rehm J. Alcohol use disorders. *Lancet*. 2019;394:781–92.
- Kauer JA, Malenka RC. Synaptic plasticity and addiction. *Nat Rev Neurosci*. 2007;8:844–58.
- You C, Vandegriff B, Brodie MS. Ethanol actions on the ventral tegmental area: novel potential targets on reward pathway neurons. *Psychopharmacology (Berl)*. 2018;235:1711–26.
- Deehan GA, Hauser SR, Wilden JA, Truitt WA, Rodd ZA. Elucidating the biological basis for the reinforcing actions of alcohol in the mesolimbic dopamine system: The role of active metabolites of alcohol. *Front Behav Neurosci*. 2013;7:104.
- Lovinger DM, Abraham KP. Synaptic plasticity mechanisms common to learning and alcohol use disorder. *Learn Mem*. 2018;25:425–34.
- Deehan GA Jr, Knight CP, Waeiss RA, Engleman EA, Toalston JE, McBride WJ, et al. Peripheral administration of ethanol results in a correlated increase in dopamine and serotonin within the posterior ventral tegmental area. *Alcohol Alcohol*. 2016;51:535–40.
- Inhibition E, Kainate OF, Neurotransmission E, The IN, Nucleus B, The OF. Ethanol inhibition of kainate receptor-mediated excitatory neurotransmission in the rat basolateral nucleus of the amygdala. *Neuropharmacology*. 2009;55:661–8.
- Weitlauf C, Woodward JJ, Carolina S, Carolina S. Ethanol selectively attenuates NMDAR-mediated synaptic transmission in the prefrontal cortex. *Alcohol Clin Exp Res*. 2008;32:690–8.
- Ramachandran B, Ahmed S, Zafar N, Dean C. Ethanol inhibits long-term potentiation in hippocampal CA1 Neurons, irrespective of lamina and stimulus strength, through neurosteroidogenesis. *Hippocampus*. 2015;25:106–18.
- Mishra D, Zhang X, Chergui K. Ethanol disrupts the mechanisms of induction of long-term potentiation in the mouse nucleus accumbens. *Alcohol Clin Exp Res*. 2012;36:2117–25.
- Wang J, Carnicella S, Phamluong K, Jeanblanc J, Ronesi JA, Chaudhri N, et al. Ethanol induces long-term facilitation of NR2B-NMDA receptor activity in the dorsal striatum: Implications for alcohol drinking behavior. *J Neurosci*. 2007;27:3593–602.
- Guan YZ, Ye JH. Ethanol blocks long-term potentiation of gabaergic synapses in the ventral tegmental area involving μ -opioid receptors. *Neuropsychopharmacology*. 2010;35:1841–9.
- Nugent FS, Penick EC, Kauer JA. Opioids block long-term potentiation of inhibitory synapses. *Nature*. 2007;446:1086–90.
- Graziane NM, Polter AM, Briand LA, Pierce RC, Kauer JA. Kappa opioid receptors regulate stress-induced cocaine seeking and synaptic plasticity. *Neuron*. 2013;77:942–54.
- Colucci-D'Amato L, Speranza L, Volpicelli F. Neurotrophic factor bdnf, physiological functions and therapeutic potential in depression, neurodegeneration and brain cancer. *Int J Mol Sci*. 2020;21:7777.
- Wang CS, Kavalali ET, Monteggia LM. BDNF signaling in context: From synaptic regulation to psychiatric disorders. *Cell*. 2022;185:62–76.
- Russo SJ, Mazei-robson MS, Ables JL, Nestler EJ. Neurotrophic factors and structural plasticity in addiction. *Neuropharmacology*. 2009;56:73–82.
- Leal G, Comprido D, Duarte CB. BDNF-induced local protein synthesis and synaptic plasticity. *Neuropharmacology*. 2014;76:639–56.
- Seroogy KB, Lundgren KH, Tran TMD, Guthrie KM, Isackson PJ, Gall CM. Dopaminergic neurons in rat ventral midbrain express brain-derived neurotrophic factor and neurotrophin-3 mRNAs. *J Comp Neurol*. 1994;342:321–34.
- Numan S, Seroogy KIMB. Expression of trk B and trk C mRNAs by adult midbrain dopamine neurons: a double-label in situ hybridization study. *J Comp Neurol*. 1999;403:295–308.
- Davis MI. Ethanol-BDNF interactions: still more questions than answers. *Pharmacol Ther*. 2008;118:36–57.
- Vargas-Perez H, Bahi A, Bufalino MR, Ting-A-Kee R, Maal-Bared G, Lam J, et al. BDNF signaling in the VTA links the drug-dependent state to drug withdrawal aversions. *J Neurosci*. 2014;34:7899–909.
- Logrip ML, Barak S, Warnault V, Ron D. Corticostriatal BDNF and alcohol addiction. *Brain Res*. 2015;1628:60–67.
- Zhang H, Xu L, Xiong J, Yang Y, Liu Y, Zhang C, et al. Role of KCC2 in the regulation of brain-derived neurotrophic factor on ethanol consumption in rats. *Mol Neurobiol*. 2023;60:1040–9.
- Li XX, Yang T, Wang N, Zhang LL, Liu X, Xu YM, et al. 7,8-Dihydroxyflavone attenuates alcohol-related behavior in rat models of alcohol consumption via TrkB in the ventral tegmental area. *Front Neurosci*. 2020;14:1–11.
- Graham DL, Edwards S, Bachtell RK, DiLeone RJ, Rios M, Self DW. Dynamic BDNF activity in nucleus accumbens with cocaine use increases self-administration and relapse. *Nat Neurosci*. 2007;10:1029–37.
- Berglind WJ, See RE, Fuchs RA, Ghee SM, Whitfield TW, Miller SW, et al. A BDNF infusion into the medial prefrontal cortex suppresses cocaine seeking in rats. *Eur J Neurosci*. 2007;26:757–66.
- Vargas-Perez H, Kee RT-A, Walton CH, Hansen DM, Razavi R, Clarke L, et al. Ventral tegmental area BDNF induces an opiate-dependent-like reward state in naïve rats. *Science*. 2009;324:1732–4.
- Santos AR, Mele M, Vaz SH, Kellermayer B, Grimaldi M, Colino-Oliveira M, et al. Differential role of the proteasome in the early and late phases of BDNF-induced facilitation of LTP. *J Neurosci*. 2015;35:3319–29.
- Pang PT, Teng HK, Zaitsev E, Woo NT, Sakata K, Zhen S, et al. Hippocampal plasticity cleavage of proBDNF by tPA / plasmin is essential for long-term hippocampal plasticity. *Science*. 2004;306:487–91.
- Vandegriff BJ, You C, Satta R, Brodie MS, Lasek AW. Estradiol increases the sensitivity of ventral tegmental area dopamine neurons to dopamine and ethanol. *PLoS ONE*. 2017;12:e0187698.
- Peris J, Steck MR, Krause EG. Oxytocin treatment for alcoholism: Potential neurocircuitry targets. *Neuropharmacology*. 2020;171:108091.
- Fontaine CJ, Patten AR, Sickmann HM, Helfer JL, Christie BR. Effects of pre-natal alcohol exposure on hippocampal synaptic plasticity: Sex, age and methodological considerations. *Neurosci Biobehav Rev*. 2016;64:12–34.
- Spear LP. Effects of adolescent alcohol consumption on the brain and behaviour. *Nat Rev Neurosci*. 2018;19:197–214.
- Wang N, Liu X, Li XT, Li XX, Ma W, Xu YM, et al. 7,8-Dihydroxyflavone alleviates anxiety-like behavior induced by chronic alcohol exposure in mice involving tropomyosin-related kinase B in the amygdala. *Mol Neurobiol*. 2021;58:92–105.
- Hogarth SJ, Jaehne EJ, van den Buuse M, Djouma E. Brain-derived neurotrophic factor (BDNF) determines a sex difference in cue-conditioned alcohol seeking in rats. *Behav Brain Res*. 2018;339:73–78.
- Halladay LR, Kocharian A, Piantadosi PT, Authement ME, Lieberman AG, Spitz NA, et al. Prefrontal regulation of punished ethanol self-administration. *Biol Psychiatry*. 2020;87:967–78.
- Rangel-Barajas C, Coronel I, Zhang Y, Hernández M, Boehm SL. Low-level developmental lead exposure does not predispose to adult alcohol self-administration, but does increase the risk of relapsing to alcohol seeking in mice: Contrasting role of GLT1 and xCT brain expression. *Neuropharmacology*. 2020;181:108339.
- Visser E, Matos MR, van der Loo RJ, Marchant NJ, de Vries TJ, Smit AB, et al. A persistent alcohol cue memory trace drives relapse to alcohol seeking after prolonged abstinence. *Sci Adv*. 2020;6:eaaax7060.
- Richardson NR, Roberts DCS. Progressive ratio schedules in drug self-administration studies in rats: a method to evaluate reinforcing efficacy. *J Neurosci Methods*. 1996;66:1–11.
- Luján MÁ, Covey DP, Young-Morrison R, Zhang L, Kim A, Morgado F, et al. Mobilization of endocannabinoids by midbrain dopamine neurons is required for the encoding of reward prediction. *Nat Commun*. 2023;14:1–12.
- St. Laurent R, Kauer J. Synaptic plasticity at inhibitory synapses in the ventral tegmental area depends upon stimulation site. *eNeuro*. 2019;6:ENEURO.0137-19.2019.

43. Wang H, Cui W, Chen W, Liu F, Dong Z, Xing G, et al. The laterodorsal tegmentum-ventral tegmental area circuit controls depression-like behaviors by activating ErbB4 in DA neurons. *Mol Psychiatry*. 2023;28:1027–45.
44. Simmons DNV, Petko AK, Paladini CA. Differential expression of long-term potentiation among identified inhibitory inputs to dopamine neurons. *J Neurophysiol*. 2017;118:1998–2008.
45. Zhang TA, Placzek AN, Dani JA. In vitro identification and electrophysiological characterization of dopamine neurons in the ventral tegmental area. *Neuropharmacology*. 2010;59:431–6.
46. Ostroumov A, Thomas AM, Kimmey BA, Karsch JS, Doyon WM, Dani JA. Stress increases ethanol self-administration via a shift toward excitatory GABA signaling in the ventral tegmental area. *Neuron*. 2016;92:493–504.
47. Inagaki T, Begum T, Reza F, Horibe S, Inaba M, Yoshimura Y, et al. Brain-derived neurotrophic factor-mediated retrograde signaling required for the induction of long-term potentiation at inhibitory synapses of visual cortical pyramidal neurons. *Neurosci Res*. 2008;61:192–200.
48. Franklin KBJ, Paxinos G *The Mouse Brain in Stereotaxic Coordinates*-3rd edition. 2008.
49. Sun YX, Su YA, Wang Q, Zheng JY, Zhang CC, Wang T, et al. The causal involvement of the BDNF-TrkB pathway in dentate gyrus in early-life stress-induced cognitive deficits in male mice. *Transl Psychiatry*. 2023;13:173.
50. Luo T-Y, Li LY, Li J, Cai S, Wang Y, Zhang L, et al. Claustrum modulates behavioral sensitivity and EEG activity of propofol anesthesia. *CNS Neurosci Ther*. 2023;29:378–89.
51. Ardinger CE, Lapish CC, Czachowski CL, Grahame NJ. A critical review of front-loading: A maladaptive drinking pattern driven by alcohol's rewarding effects. *Alcohol Clin Exp Res*. 2022;46:1772–82.
52. Zucker RS, Regehr WG. Short-term synaptic plasticity. *Annu Rev Physiol*. 2002;64:355–405.
53. Yang Y, Calakos N. Presynaptic long-term plasticity. *Front Synaptic Neurosci*. 2013;5:8.
54. Wise RA, Jordan CJ. Dopamine, behavior, and addiction. *J Biomed Sci*. 2021;28:1–9.
55. Palmiter RD. Dopamine signaling in the dorsal striatum is essential for motivated behaviors: lessons from dopamine-deficient mice. *Ann N Y Acad Sci*. 2008;1129:35–46.
56. Komatsu Y. GABA B receptors, monoamine receptors, and postsynaptic inositol trisphosphate-induced Ca^{2+} release are involved in the induction of long-term potentiation at visual cortical inhibitory synapses. *J Neurosci*. 1996;16:6342–52.
57. Nugent FS, Niehaus JL, Kauer JA. PKG and PKA signaling in LTP at GABAergic synapses. *Neuropsychopharmacology*. 2009;34:1829–42.
58. Liu Y, Koo JS, Zhang H. Chronic intermittent ethanol exposure-induced m6A modifications around mRNA stop codons of opioid receptor genes. *Epigenetics*. 2024;19:2294515.
59. Cai CY, Chen C, Zhou Y, Han Z, Qin C, Cao B, et al. PSD-95-nNOS coupling regulates contextual fear extinction in the dorsal CA3. *Sci Rep*. 2018;8:4–15.
60. Biojone C, Casarotto P, Cannarozzo C, Fred SM, Herrera-Rodríguez R, Lesnikova A, et al. nNOS-induced tyrosine nitration of TRKB impairs BDNF signaling and restrains neuronal plasticity. *Prog Neurobiol*. 2023;222:102413.
61. Lan L, Wang H, Zhang X, Shen Q, Li X, He L, et al. Chronic exposure of alcohol triggers microglia-mediated synaptic elimination inducing cognitive impairment. *Exp Neurol*. 2022;353:114061.
62. Cheng Q, Song SH, Augustine GJ. Calcium-dependent and synapsin-dependent pathways for the presynaptic actions of BDNF. *Front Cell Neurosci*. 2017;11:75.
63. Jackson RE, Burrone J. Visualizing presynaptic calcium dynamics and vesicle fusion with a single genetically encoded reporter at individual synapses. *Front Synaptic Neurosci*. 2016;8:21.
64. Koob GF. Animal models of craving for ethanol. *Addiction*. 2000;95:573–81.
65. Roberto M, Nelson TE, Ur CL, Gruol DL. Long-term potentiation in the rat hippocampus is reversibly depressed by chronic intermittent ethanol exposure. *J Neurophysiol*. 2002;87:2385–97.
66. Heberlein A, Büscher P, Schuster R, Kleimann A, Lichtiginghagen R, Rhein M, et al. Do changes in the BDNF promoter methylation indicate the risk of alcohol relapse? *Eur Neuropsychopharmacol*. 2015;25:1892–7.
67. Lacroix A, Ramoz N, Girard M, Plansont B, Poupon D, Gorwood P, et al. BDNF CpG methylation and serum levels covary during alcohol withdrawal in patients with alcohol use disorder: A pilot study. *World J Biol Psychiatry*. 2023;24:854–9.
68. Han J, Park H. Recycling of endocytic BDNF through extracellular vesicles in astrocytes. *Sci Rep*. 2025;15:2011.
69. Marshall SA, McClain JA, Wooden JI, Nixon K. Microglia dystrophy following binge-like alcohol exposure in adolescent and adult male rats. *Front Neuroanat*. 2020;14:52.
70. Liu JH, Zhang M, Wang Q, Wu DY, Jie W, Hu NY, et al. Distinct roles of astroglia and neurons in synaptic plasticity and memory. *Mol Psychiatry*. 2022;27:873–85.
71. Friend LN, Wu B, Edwards JG. Acute cocaine exposure occludes long-term depression in ventral tegmental area GABA neurons. *Neurochem Int*. 2021;145:105002.
72. Valyear MD, Glovaci I, Zaari A, Lahlou S, Trujillo-Pisanty I, Andrew Chapman C, et al. Dissociable mesolimbic dopamine circuits control responding triggered by alcohol-predictive discrete cues and contexts. *Nat Commun*. 2020;11:3764.
73. Ma T, Cheng Y, Roltsch Hellard E, Wang X, Lu J, Gao X, et al. Bidirectional and long-lasting control of alcohol-seeking behavior by corticostriatal LTP and LTD. *Nat Neurosci*. 2018;21:373–83.
74. Chen BT, Bowers MS, Martin M, Hopf FW, Guillory AM, Carelli RM, et al. Cocaine but not natural reward self-administration nor passive cocaine infusion produces persistent LTP in the VTA. *Neuron*. 2008;59:288–97.
75. Wu YC, Hill RA, Gogos A, Van Den Buuse M. Sex differences and the role of estrogen in animal models of schizophrenia: Interaction with BDNF. *Neuroscience*. 2013;239:67–83.
76. Hilderbrand ER, Lasek AW. Studying sex differences in animal models of addiction: an emphasis on alcohol-related behaviors. *ACS Chem Neurosci*. 2018;9:1907–16.
77. Polter AM, Barcomb K, Tsuda AC, Kauer JA. Synaptic function and plasticity in identified inhibitory inputs onto VTA dopamine neurons. *Eur J Neurosci*. 2018;47:1208–18.
78. Soares-Cunha C, Domingues AV, Correia R, Coimbra B, Vieitas-Gaspar N, de Vasconcelos NAP, et al. Distinct role of nucleus accumbens D2-MSN projections to ventral pallidum in different phases of motivated behavior. *Cell Rep*. 2022;38:110380.
79. Zachry JE, Kutlu MG, Yoon HJ, Leonard MZ, Chevée M, Patel DD, et al. D1 and D2 medium spiny neurons in the nucleus accumbens core have distinct and valence-independent roles in learning. *Neuron*. 2024;112:835–49.e7.
80. Abraham KP, Salinas AG, Lovinger DM. Alcohol and the brain: neuronal molecular targets, synapses, and circuits. *Neuron*. 2017;96:1223–38.

ACKNOWLEDGEMENTS

This work was supported by the Key Project of the Heilongjiang Natural Science Foundation (ZD2022H007 to Y.Z.G.); the National Natural Science Foundation of China (81871041 to Y.Z.G.) and Mudanjiang Key R&D Program Project (XDHD25CR018 to Y.Z.G.).

AUTHOR CONTRIBUTIONS

YG, JX and XZ designed the study. JX, MD, XQ, DC, HD, CD, XX, XW, JW, and XS contributed to data collection and conducted all surgeries and behavior studies. JX contributed to electrophysiological experiments, fiber photometry, and immunohistochemistry experiments. MD, JW and XS contributed to Western blot experiments. JX analyzed all the data and wrote the paper. JX, YG, YW and TZ revised the manuscript. YG supervised the study and obtained the funding.

COMPETING INTERESTS

The authors report no biomedical, financial, or other potential conflicts of interest.

ADDITIONAL INFORMATION

Supplementary information The online version contains supplementary material available at <https://doi.org/10.1038/s41380-026-03532-4>.

Correspondence and requests for materials should be addressed to Yanzhong Guan.

Reprints and permission information is available at <http://www.nature.com/reprints>

Publisher's note Springer Nature remains neutral with regard to jurisdictional claims in published maps and institutional affiliations.



Open Access This article is licensed under a Creative Commons Attribution-NonCommercial-NoDerivatives 4.0 International License, which permits any non-commercial use, sharing, distribution and reproduction in any medium or format, as long as you give appropriate credit to the original author(s) and the source, provide a link to the Creative Commons licence, and indicate if you modified the licensed material. You do not have permission under this licence to share adapted material derived from this article or parts of it. The images or other third party material in this article are included in the article's Creative Commons licence, unless indicated otherwise in a credit line to the material. If material is not included in the article's Creative Commons licence and your intended use is not permitted by statutory regulation or exceeds the permitted use, you will need to obtain permission directly from the copyright holder. To view a copy of this licence, visit <http://creativecommons.org/licenses/by-nc-nd/4.0/>.